Editorial Manager(tm) for The Geological Society of America Bulletin
Manuscript Draft

Manuscript Number:

Title: A Relict Paleoseismic Record of Seven Earthquakes between 600 AD and 2000 BC on the Central North Anatolian Fault at Elmacik, near Osmancik, Turkey.

Short Title: A Relict Paleoseismic Record of Seven Earthquakes between 600 AD and 2000 BC on the Central North Anatolian Fault at Elmacik, near Osmancik, Turkey.

Article Type: Article

Keywords: North Anatolian Fault, Paleoseismology, slip-rate, sedimentary sequence, shattered landscape, Hattusas

Corresponding Author: Mr Jeffrey Fraser,

Corresponding Author's Institution: Royal Observatory of Belgium

First Author: Jeffrey Fraser

Order of Authors: Jeffrey Fraser; Aurelia Hubert-Ferrari; Kris Vanneste; Sevgi Altinok; Laureen Drab

Abstract: Deformation along the northern edge of the westward moving Anatolian Plate is concentrated along the North Anatolian Fault (NAF). The northward arching NAF extends from the Karliova triple junction in the east, ~1500 km into the Aegean Sea in the east. A sequence of twentieth century earthquakes ruptured the NAF displaying a spatiotemporal pattern consistent with a prominent stress triggering mechanism. In 1943 the M 7.6 Tosya earthquake ruptured a 280 km segment of the central portion of the NAF. Four paleoseismic investigations have previously studied this segment of the fault and this study was conducted near its centre. A paleoseismic trench revealed a sequence of eight sediment packages abutting a highly developed discrete shear zone. Each of the packages comprised a fine-grained layer overlying a coarse layer. We interpret that the coarse layers are deposited in response to earthquakes due to increased erosion on an adjacent steep slope. The youngest event horizon correlates to the historical 529AD earthquake. Timing of six older earthquakes is constrained to (2σ); 23BC-103AD, 609-185BC, 971-814BC, 1227-968BC, 2050-1777BC, and 2556-2235BC, which corresponds to a summed inter-event time of 97-912 years. The earthquake record is relict because the local stream network incised around 1000AD isolating the trench site from the adjacent steep slope. A stream adjacent to the trench site has subsequently been offset by 23.5±1.5 m yielding a right-lateral slip-rate of 21.4-25.6 mm/yr and indicating that the 1943 rupture caused an uncharacteristically small offset.

Suggested Reviewers: Jim Lienkaemper
jlienk@usgs.gov
Jim has edited a recently accepted paper of ours in the Bulletin of the Seismological Society of America and provided very useful feedback. I think he may also find this interesting.

james Dolan
dolan@usc.edu
An extensive background in paleoseismology research in particular on the North Anatolian Fault.

Opposed Reviewers:

Cover Letter

Click here to download Cover Letter: J.Fraser.doc

A Relict Paleoseismic Record of Seven Earthquakes between 600 AD and 2000 BC on the Central North Anatolian Fault at Elmacik, near Osmancik, Turkey.

J. Fraser[1], A. Hubert-Ferrari[1,2], K. Vanneste[1], S. Altinok[3], L. Drab[2]
1:Seismology Section, Royal Observatory of Belgium, Avenue Circulaire 3, 1180 Brussels, Belgium
2: CNRS, Laboratorie de Geologie UMR 8538, Ecole Normale Superieure, 24 Rue Lhomond, 75231, Paris CEDEX 5, France
2: Osmangazi University, Engeneering Faculty, Dept. of Geology, Eskisehir, Turkey

Key words: North Anatolian Fault, Paleoseismology, slip-rate, sedimentary sequence, shattered landscape, Hattusas.

Abstract (250 words)

Deformation along the northern edge of the westward moving Anatolian Plate is concentrated along the North Anatolian Fault (NAF). The northward arching NAF extends from the Karliova triple junction in the east, ~1500 km into the Aegean Sea in the east. A sequence of twentieth century earthquakes ruptured the NAF displaying a spatiotemporal pattern consistent with a prominent stress triggering mechanism. In 1943 the M 7.6 Tosya earthquake ruptured a 280 km segment of the central portion of the NAF. Four paleoseismic investigations have previously studied this segment of the fault and this study was conducted near its centre. A paleoseismic trench revealed a sequence of eight sediment packages abutting a highly developed discrete shear zone. Each of the packages comprised a fine-grained layer overlying a coarse layer. We interpret that the coarse layers are deposited in response to earthquakes due to increased erosion on an adjacent steep slope. The youngest event horizon correlates to the historical 529AD earthquake. Timing of six older earthquakes is constrained to (2σ); 23BC–103AD, 609–185BC, 971–814BC, 1227–968BC, 2050–1777BC, and 2556–2235BC, which corresponds to a summed inter-event time of 97–912 years. The earthquake record is relict because the local stream network incised around 1000AD isolating the trench site from the adjacent steep slope. A stream adjacent to the trench site has subsequently been offset by 23.5±1.5 m yielding a right-lateral slip-rate of 21.4–25.6 mm/yr and indicating that the 1943 rupture caused an uncharacteristically small offset.

Introduction

The North Anatolian Fault (NAF) is an approximately 1500 km long, right-lateral, strike-slip plate boundary fault which arcs across the north of modern Turkey (Fig. 1a). Twentieth century earthquakes on the NAF ruptured in an apparently migrating sequence of large, destructive earthquakes from east to west (i.e. Barka, 1992; Barka and Kadinsky-Cade, 1988; Stein et al., 1997). This pattern of migrating earthquakes indicates a strong relationship between fault rupture and increased risk of rupture on adjacent strands of the NAF. Because the latest earthquake in the migrating sequence occurred at the edge of the Marmara Sea, near Istanbul, the possible westward continuity of the sequence involves a very significant hazard to one of the most populous cities in the world. The migrating earthquake sequence suggests that the NAF is a relatively simple fault system which responds to accumulated stress by a cascading exceedance of stress thresholds triggered by a pulse of strain on an adjacent fault segment(s). By improving our understanding of this relatively simple fault system, our understanding of why and when faults give rise to earthquakes can be enhanced.

A long historical record of many surface-rupturing earthquakes documents extensive destruction and loss of life along the NAF. The historical records provide precise temporal constraints of earthquakes during about the last 2000 years. An ever increasing number of paleoseismic investigations have been undertaken on the NAF and these strongly suggest that the historical earthquake record is incomplete, particularly in the central sections of the fault. Additionally, the historical earthquake record provides little spatial constraint on the location of surface rupture.

The 1943 Tosya earthquake ruptured a 280 km segment of the NAF including through this study area (Fig. 1). Paleoseismic investigations have been conducted on this segment of the NAF at four sites: Ilgaz (Sugai et al., 1999), Havza (Yoshioka et al., 2000), Alayurt (Hartleb et al., 2003), and Destek (Fraser et al., 2009). The largest distance between existing paleosesimic investigations on the 1943 rupture segment lies between Ilgaz and Havza. In this study we describe a paleoseismic record of 7 earthquakes at Elmacik approximately 65 km west of Havza, and 115km east of Ilgaz.

Seismotectonic Setting

The Anatolian plate is a small piece of continental plate which is rotating anticlockwise as it escapes westward relative to the Eurasian plate. The translation and deformation of

the Anatolian plate is facilitated by 3 fundamental tectonic forces relative to a stable Eurasia; 1) a pushing force exerted by the northward drifting Arabian plate (synonymous with lateral escape or extrusion) (Barka and Kadinsky-Cade, 1988; Flerit et al., 2004; Hubert-Ferrari et al., 2002), 2) a pulling force from extension in the western portion of the plate due to back-arc extension associated with the Hellenic subduction zone (Flerit et al., 2004), and 3) to some degree a dragging force exerted on the Anatolian plate from below the lithosphere (Westaway, 2003). The North Anatolian Fault (NAF) is the northern margin of the Anatolian plate along which the dextral strike-slip deformation associated with westward escape is concentrated. The southeast side of the Anatolian plate is bounded by the East Anatolian Fault (EAF) which accommodates most the left lateral strike-slip displacement on this side of the plate. The western end of the NAF extends into the Aegean extensional domain. The Aegean extensional domain extends across most of the western half of the Anatolian plate and is attributed to back arc extension in response to subduction processes at the Hellenic subduction zone (Flerit et al., 2004). Interaction of the extensional regime in the western Anatolian plate with the western portion of the strike-slip NAF (west of approximately Bolu) may explain why fault ruptures on this section are shorter and temporally dispersed relative to the eastern portion (Pondard et al., 2007).

The NAF follows a path that is coincident with former compressive structures such as the Anatolide-Pontide suture (Barka et al., 2000) and the preliminary stage of fault propagation gave rise to a series of fault-splay related sedimentary basins which were predominantly bypassed to form the NAF. As a consequence of this complex history, it is difficult to constrain the total offset or age of the NAF. Hubert-Ferrari et al (2002) identified several large offset features in the vicinity of this study including the 80 km offset of the proto Tosya-Vezirkopru basins, a 30 km offset of the Kizilirmak River, and a 75 km offset of the proto Yesilirmak River. The 80 km of total offset on this section of the NAF is consistent with the total offset recorded by the geometries of the Tasova-Erbaa and Niksar pull-apart basins which are situated at the eastern end of the 1943 Tosya Earthquake rupture (Barka et al., 2000).

Detailed geomorphic studies at the Eksik and Bersin basins near Ilgaz, approximately 90km west of Elmacik, were undertaken by Hubert-Ferrari et al (2002) following the

identification of offset valley systems by Barka and Hancock (1984). They found a common ~200m offset of deeply incised fluvial surfaces which they attributed to the post-glacial downcutting beginning around 10 – 12 ka, implying a long-term slip-rate of 18.5 ± 3.2 mm/yr (this typical offset has been recognized at several locations along the NAF). In the Bersin basin, offset younger deposits gave a slip-rate of 12.5 – 23 mm/yr over the last few thousand years. Kozaci et al (2007) subsequently undertook a study of younger sediments in the Eksik basin and determined a slip-rate of 19 ± 7 mm/yr over the last 2.1 – 2.9 ka and 25.5 ± 9.5 mm/yr over the last 1.6 – 2.2 ka. In another study, at Tahtakopru, in the Koca R. valley approximately 13 km east along the NAF from the principal trench in this study, Kozaci et al (Kozaci et al., 2009) defined a preferred slip-rate of 18.6 +3.5/-3.3 mm/yr over the last ~3 ka using cosmogenic nuclide dating of a surface with an incised stream offset by 55±10 m.

Using the GPS velocity field, Relinger et al (2006) constrained the rates and styles of displacement using a block model. The block model considered the 1943 Tosya earthquake rupture segment as part of 2 straight lines, an eastern line with a strike of ~106° and a western line with a strike of ~78°. The model gives the eastern line a right-lateral displacement rate of 25.8 ± 0.2 mm/yr with a relatively insignificant extensional fault-normal rate of 0.2 ± 0.2 mm/yr. The western line has a modeled right-lateral displacement rate of 24.2 ± 0.2 mm/yr, and a large compressional fault-normal rate of 8.0 ± 0.2 mm/yr. The NAF has a strike of approximately 93° in our study area which is near the junction of the 2 line segments used in the GPS block model of Relinger et al (2006), therefore the local GPS block model derived right-lateral slip-rate is in the order of 25 ± 1 mm/yr with some amount of fault-normal movement. Flerit et al (2004) use an elastic block model (i.e. accommodates some deformation within the blocks) which has a more realistic strike for this segment of the fault. This model yields a right-lateral slip-rate of 24 mm/yr with 3 mm/yr of fault-normal extension. Therefore, the local slip-rate based on GPS measurements is about 24.5 ± 1.5 mm/yr and the fault-normal displacement rate is probably about an order of magnitude lower and could be either compressional or extensional.

The Historical Earthquake Record

During the 20th century a sequence of large surface-rupturing earthquakes ruptured almost the entire NAF. Between 1939 and 1943 earthquakes ruptured ~725km of the NAF with a westward progression (Stein et al., 1997) (Fig. 1a). Subsequently this cascading pattern has migrated both east and west with the most recent surface-rupturing events occurring in 1999 near the eastern side of the Marmara Sea. This pattern of faulting is attributed to a relatively constant accumulation of strain along the fault and an associated triggering pulse of stress caused by strain on an adjacent strand(s). The simple pattern of earthquakes, particularly on the segments which ruptured between 1939 and 1943, can be attributed to the simple fault geometry with very few other major structures interacting with the NAF in conjunction with a relatively high level of accumulated stress.

The central segment of the NAF, the segment on which we focus, ruptured for 280 km along strike in the magnitude 7.6, 1943 Tosya Earthquake (Barka, 1996). The distribution of right-lateral displacements caused by the 1943 earthquake has a "saddle-like" geometry with maximum displacement of about 4.5 m toward the west and generally decreasing to the east, except for a spike near Lake Ladik (Fig. 1c) (Barka, 1996). Approximately 11 km west of the trench site, near the village of Kamil, offsets varied from 1.4 m to 2.6 m of right-lateral displacement (Barka, 1996). A geomorphic study approximately 90 km west of Elmacik (Kozaci et al., 2007) concluded that the 4 – 4.5 m displacement caused by the 1943 earthquake locally, which is significantly larger than the offset near Kamil, was anomalously small.

Prior to the 1943 earthquake, there is considerably more doubt about which fault segments ruptured to cause the damage that generally features in the historical records. Historical earthquake records prior to approximately the last 100 years are almost never fault specific. Hereafter, all historical records which may correspond to complete or partial rupture of the 1943 rupture segment of the NAF are described. On June 25 1910 AD an earthquake occurred near Osmacik (Ambraseys, 2001; Ambraseys and Finkel, 1987) however, the M: 6.1 event was probably too small to have caused surface rupture. On 18 July 1794 AD an event caused major damage in Corum (a major city approximately 50 km south of Osmancik) and significant effects in Amasya and possibly Havza (there is some confusion in translation) (Ambraseys and Finkel, 1995). It is

possible that this 1794 AD earthquake ruptured part of the Tosya earthquake rupture segment, however the spatially limited reports suggest it was not laterally extensive. On 29 December 1776 AD an earthquake caused damage to Amasya, Merzifon, and Vezirkopru. About 100 lives were lost at the latter two locations (Ambraseys and Finkel, 1995). This 1776 AD earthquake may have been a partial rupture of the Tosya earthquake rupture segment; however we speculate that the limited spatial extent of reports suggests that it probably did not cause surface rupture.

1668 AD was a big year for earthquakes on the North Anatolian Fault (Ambraseys and Finkel, 1995; Ambraseys and Jackson, 1998; Sengor et al., 2005). A long sequence of damaging earthquakes beginning in late June 1668 AD was reported in Ankara and continued until 20 July causing extensive damage and some deaths. After 20 July the intensity of the earthquakes began to increase and on 12 August a violent shock was felt in Istanbul. Earthquakes continued to intensify until 15 August when a very large earthquake caused further major damage to Ankara. On 17 August 1668 AD the largest earthquake of the sequence, and possibly the largest historical earthquake on the entire NAF, occurred. This 17 August earthquake affected Ankara, Beypazari, Bolu, Kastamonu, Ilgaz, Havza, Amasya, Tosya, Tokat, Erzincan, and Zara amongst other settlements (Ambraseys and Finkel, 1995). The 17 august 1668 AD earthquake almost certainly ruptured the Tosya Earthquake rupture segment and possibly more of the NAF. Which segments of the NAF or other less active structures in the Anatolian plate ruptured to give rise to the main shocks and prolonged sequence of earthquakes in 1668 AD remains uncertain, particularly the role of major asperities on the fault such as the Niksar pull-apart basin.

In 1598 AD an earthquake reportedly killed 60000 men in central north Anatolia, including the city of Amasya, and possibly generated a tsunami on the Black Sea coast (Ambraseys and Finkel, 1995). This earthquake may have involved rupture of the NAF however, the spatial constraints are too vague to identify on which segments. An earthquake caused an unclear degree of damage to Amasya in 1590 AD (Ambraseys and Finkel, 1995), the limited extent of reports suggests to us that this earthquake probably did not involve surface-rupture of the NAF. An earthquake in 1579 AD reportedly caused damage in the Corum to Amasya area and probably the Erzincan region (Ambraseys and

Finkel, 1995). We speculate that, since there are no reports from the regions between Amasya and Erzincan, the 1579 AD event may reflect two separate earthquakes which probably were not associated with surface rupture. In a similar way an earthquake in 1543 AD which caused the collapse of 30 houses in Corum and the demolition of Erzincan (Ambraseys and Finkel, 1995), is probably not associated with a single surface rupture, and the destruction in Corum could have been caused by an earthquake that did not rupture the surface. An earthquake in 1050 AD was reported near Cankiri (~10 km south of Ilgaz). Although a great deal of damage was caused by an associated landslide-dam failure it is not clear if this earthquake was large enough to have caused surface rupture (Ambraseys and Jackson, 1998; Guidoboni and Comastri, 2005). An earthquake around 1035 AD (between 1 September 1034 AD and 31 August 1035 AD) destroyed 5 unknown villages in northern Turkey not including Ankara, this vague report probably correlates to a surface-rupturing earthquake but it is not obvious which segment(s) ruptured (Ambraseys and Jackson, 1998; Guidoboni and Comastri, 2005). In 529 AD (possibly July) a vague report of suffering in Amasya may reflect an earthquake (Guidoboni et al., 1994). In 235 or 236 AD an earthquake occurred near Amasya which killed at least one child for which a grave-stone inscription attributes his death to an earthquake. Additionally, this event is mentioned in a text from further away suggesting that it was a significant earthquake (Guidoboni et al., 1994).

Historical evidence of earthquakes older than 2000 years is very scant indeed, however it has been postulated that the collapse of many ancient cities in the period 1225 – 1175 BC was caused by a "storm" of earthquakes in the Aegean and Eastern Mediterranean region (Nur and Burgess, 2008; Nur and Cline, 2000), although not all agree (i.e. Drews, 1993). During this widespread destruction the ancient cities of Hattusas, Karaoglan, Alishar Hoyuk, and Musat amongst many other cities, were destroyed (Nur and Cline, 2000) (Fig. 1a). Nur and Cline (2000) speculate that an earthquake similar in magnitude to the 1668 AD earthquake could have been, directly or indirectly, responsible for this. The distribution of these cities is consistent with a possible rupture of the 1943 rupture segment.

Pre-existing Paleoseismic investigations

Many paleoseismic investigations have been undertaken on the NAF but for simplicity we focus on studies undertaken at Ilgaz (Sugai et al., 1999), Havza (Yoshioka et al., 2000), Alayurt (Hartleb et al., 2003), and Destek (Fraser et al., 2009) which are also situated on the 1943 rupture segment of the NAF (Fig. 1b). We have reanalyzed the available dating data from each of these studies using Bayesian ordering constraints. Because this data is compared to the results from this study it is described in the discussion.

We went to the field in 2008 with the goal of studying an area between prior paleoseismic investigations at Ilgaz (Sugai et al., 1999) and Havza (Yoshioka et al., 2000) as this is one of the longest unstudied sections of the NAF (Fig. 1b). After several days of reconnaissance in early April 2008 a study area with an abundance of sites with potential to yield long paleoseismic records was selected (Fig. 2). Field work was performed during June and July 2008.

Study Area Tectonic Geomorphology

At the western end of the field area the meandering Kizil R. (Kizilirmak), associated alluvial terraces, and tributary stream alluvial fan surfaces dominate the valley floor geomorphology (Fig. 2). This natural geomorphology has been largely overprinted by ongoing intensive rice cultivation. There are many hill peaks and relict surfaces about 70m above the active flood plain which we interpret as a paleo-valley floor. In some places this surface is comprised of eroded rock and in others river gravel. We speculate that these surfaces may have been abandoned around the end of the last glacial period 10 – 12 ka ago like the older surfaces identified at Eksik (Hubert-Ferrari et al., 2002). Mountain ranges to the north and south of the fault strike East-West parallel to the fault. The south-facing slopes tend to be actively eroding and less vegetated while the north-facing slopes are more vegetated and have less extensive active erosion. The differences in geomorphology between the north and south aspects are attributed to some combination of sunshine, precipitation, vegetation, and geology.

East of the Kizil R. the geomorphology is dominated by the Zeytin R. which drains westward from a valley comprising most of the field area into the Kizil R. The main channel of the Zeytin R. is broad and braided, although it only flows after significant rainfall or the annual snow melt. Extensive stream incision and reactivation of landscape

is evident in all orders of drainage. This suggests that the Kizil R. has been incising, however a Paphalagonian rock-cut tomb is situated very near the Kizil R. Level (Fig. 3). Paphalagonian rock-cut tombs were constructed from the early 5th century BC to the 3rd century AD, therefore river level has been nearly static for approximately the last 2000 years (von Gall, 1966 in Matthews, 2009). Tributaries to the Zeytin R., show patterns of incision where several phases of knick-point propagation can be recognized in the stream bed geomorphology and the adjacent landscape activity. We propose a few possible causes of this; 1) tectonics; fault offsets cause steps in stream profiles, 2) erosion of the Zeytin R. banks trims alluvial fans causing local base-level incision in tributary stream profiles, and 3) it is possible that the pattern of incision reflects the pre-2000-year incision of the Kizil R. which is still spreading through the drainage basin. Another possibility is that the voluminous and extensive landslide south of the Zeytin R. between Hanefi and Kuzalibey has been incrementally blocking the river then eroding causing fluctuations in stream profiles. Although a plausible cause there is significant erosion downstream of the landslide, so this is certainly not the only cause of incision.

Throughout the field area the location of faults is relatively well constrained by distributed geomorphic features and descriptions by locals of the 1943 fault rupture (notably, this is never first-hand knowledge). West of the Kizil R. the fault is very linear and forms a single continuous trace, although it is not clearly identifiable in the distal part of alluvial fans due to rice cultivation. Where the fault crosses hill terrain, streams are offset by various amounts and where it crosses the fan surface it has a very clear scarp with a down to the south displacement. On the east side of the river intensive rice cultivation also hides the fault trace.

At the village of Kamil a right-stepping releasing step-over with a step-over-distance of approximately 1 km was identified. In the absence of a pre-existing name we propose to name the basin the Kamil pull-apart basin (KPAB). It splits the fault segment "Fs20" identified by Barka and Kadinsky-Cade (1988) into two possible segments labeled S3 and S4 on Figure 1c. The fault traces are incomplete on the fans due to a high rate of avulsion, and in other places due to farming and overprinting of the trace by the village of Kamil. However, enough clear fault traces were recognized to distinguish a series of four northwest-arching horse-tail splays running into the pull-apart basin from the fault trace

which continues to the east. This interpretation of fault geometry is consistent with reports from locals who showed us where fault ruptures occurred during the 1943 earthquake. The significant ~1 km step-over-distance is unlikely to arrest fault rupture (Lettis et al., 2002) but may play a role in fault-rupture propagation.

East of the KPAB the NAF forms a single active trace which is seldom evidenced on the valley floors due to the high rates of sedimentation and erosion. There are many offset streams and ridges, captured streams, side-hill benches and upslope- and downslope-facing fault scarps. East of the trench site (Fig. 2) the fault steps up onto a higher side-hill bench with deeply incised and offset streams. At the high pass between the drainage basin associated with Zeytin R. and the east draining Koca R. (Koca Cay) there is a small, lake filled (Kunduz L.), releasing step-over with a step-over-distance of approximately 200 m. The lake has been modified by people but the formation of the depression is clearly caused by active faulting. East of Kunduz L. the fault trace is 1 single strand for about 1.5 km before it splits into at least 2 active strands at the eastern end of the study area (Fig. 2). To the edge of the study area the landscape is similar to the other side of the Kunduz L. with the fault trace causing upslope-facing scarps on a side-hill bench and offsetting streams and ridges.

Paleoseismic Investigation

Trench Site Selection

To select a paleoseismic trenching location we walked over the field area to identify sites with the potential to yield long paleoearthquake records. The second phase of trench-site selection was test pitting during which a backhoe excavated test pits approximately 2 m deep and 2 m wide and usually 10 m long to expose the soil profile on both sides of the fault.

Test pit TP1 (Fig. 2) was excavated across an ~5 m high down-slope- and south-facing scarp. Several fault planes were revealed by means of aligned clasts, but the strata were crude and gravelly without fine-grained matrix, meaning the test pit was not particularly interesting or stable. Test pit TP2 was excavated across a 1.5-2.0 m high south-facing scarp on an alluvial fan as close as possible to the rice fields which occupy the distal part of the fan surface. TP2 revealed gravelly strata and was very unstable. This test pit was abandoned for the same reason as TP1. Test pits TP3, TP5, and TP6 were excavated across clear up slope facing fault scarps and all revealed detailed stratigraphy with fine

gravels and silty sands, but only one offset was evident which may have been caused by more than one earthquake. Test pit TP4 revealed no fault and a re-interpretation of the site led us to change what was considered a fault scarp into a recent stream terrace riser. Test pits TP7 and TP8 were excavated on the elevated side-hill bench situated east of Kunduz L. TP7 was excavated across an upslope-facing scarp which had captured, or possibly offset, a small stream. The trench revealed relatively simple organic rich strata which showed evidence for 1 offset, although this may have been the result of more than 1 earthquake rupture. TP8 was opened on the edge of an offset ridge where it was expected that successive events would generate an unstable fault scarp and perhaps colluviums would be intermittently deposited across the fault. The test pit revealed fault-zone melange on the northern relatively up-thrown side of the fault and wedges of boulders on the down-thrown side of the fault. Unfortunately, an absence of any other source of materials during the inter-event period rendered these wedges indistinguishable from each other and undateable. The ninth test pit was expanded into the principal paleoseismic trench which is the focus of this paper.

Trench Site Geomorphology

The trench site geomorphology is principally comprised of a steep north-facing slope with a relatively flat area at its base (Fig. 3). This flat area is referred to as a side-hill bench as it forms a terrace, with the exception of a subtle ridge along the northern edge. The main strand of the NAF locally traces along the southern edge of the ridge which bounds the side-hill bench. A valley runs down the steep north-facing slope and from its base a small channel is incised into the side-hill bench, for ease of discussion we call this the YY channel. The YY channel has a steep ~2.1 ha drainage basin area. The YY channel drains into a northward flowing, deeply incised (~15 m) stream (XX stream) that is offset by the fault and has a steep ~35 ha drainage basin area. In Figure 3a the fault is comprised of a series of three en echelon (left-stepping) strike-slip faults which offset geomorphic features. Near the edges of Figure 3a the fault strands are not recognizable in the geomorphology which is attributed to localized high rates of erosion. The paleoseismic trench was excavated across the fault trace where it forms the southern side of the ridge which bounds the side-hill bench.

To determine when the YY channel incised into the side-hill bench a small pit was excavated into the surface of a relict channel form near the XX stream to collect a charcoal sample for radiocarbon dating ("surface sample" Fig. 3d). It is more interesting to consider the dating result with the dates obtained near the surface in the trench, so the evolution of the trench site geomorphology is described in the event chronology section.

Trenching procedure

The test pit was expanded into a trench using the front (big) bucket of the backhoe down to a maximum depth of ~3 m then the back hoe (little bucket) excavated another trench down to maximum depth of ~6 m below the surface leaving a bench separating upper and lower walls on both sides of the trench. The trench walls were scraped clean before attaching a 1 x 1 m string grid. Using a coordinate system established with an origin (horizontal (H) 0 m and vertical (V) 0 m) in the bottom north corner of the trench the nature and distribution of sediments exposed in the trench were described. Following the same methodology used at Destek (Fraser et al., 2009) the magnetic susceptibility of a swath of the east wall between H:8.9 and H:10.9 on the upper wall and H:9.9 and H:11.9 on the lower wall was logged. After logging, samples were collected to provide age constraints on the earthquake event horizons. We employed a charcoal sampling strategy that may be applied in other trenches with similar sediments (Electronic supplement 1). 170 samples of charcoal were collected from the trench. The trench log (Fig. 4) is presented with abbreviated unit descriptions, the unit labels correspond to a more detailed set of soil descriptions (Electronic supplement 2).

Trench Stratigraphy

The trench logs (Fig. 4a.b.c) reveal a sandy cobbly river gravel with very little bedding north of a well developed and very poorly sorted clayey gravel shear zone that extends right to the base of the plough zone. South of the shear zone a repetitive sequence of 8 packages each comprising two layers; an upper layer of fine-grained (clay - fine sand) sediments with some gravel, over a lower layer of coarser sediments (gravel and cobbles) with a fine-grained matrix, were exposed. On the upper east wall of the trench there is a zone of highly deformed and altered layers which are obviously a bulb of deformation associated with, now absent, tree roots.

The magnetic susceptibility logging (Fig. 4d) did not yield any useful results. All of the values are less than 40 (SI. dimensionless) which is considerably lower than the values encountered in the study at Destek (Fraser et al., 2009). Because of the lack of contrast in the results these data are not discussed further.

Event Stratigraphy

Conventional methods of identifying the occurrence of earthquakes in paleoseismic trenches on strike-slip faults include identifying upward fault terminations, varying amounts of deformation, and colluvial wedges. In this trench these structural features are not recognized. The trench stratigraphy suggests that there is a small, but consistent, down to the south component of displacement locally. When this section of the fault ruptures a small upslope-facing scarp is formed which creates a sediment trap. We infer that the stratigraphy in the sediment trap, on the south side of the fault shear-zone, reflects the timing of earthquakes because of the effect of earthquakes on erosion of the steep slope to the south of the trench which is now the catchment of the YY channel. This interpretation is consistent with field observations of Keefer and Moseley (2004) who visited the damage zone of the 23 June 2001 southern Peru earthquake (M_w: 8.2 – 8.4) and described "…seismic shattering of the landscape detaches vast amounts of loose material from hillsides and channel banks, thereby increasing the amount of sediment available for transport…" (p. 10881, Keefer and Moseley, 2004). However, in this case we infer that such consequences are limited to very steep slopes, such as that south of the trench site.

Because of the strong ground shaking caused by fault rupture in conjunction with the steep slope angle many small scale slope failures occur, cracks become dilated, the banks of the steep channel on the slope collapse, and trees probably fall over. After the earthquake event there is an abundance of loose materials on the slopes. During subsequent rainfall events, or more likely at this location during the spring snow melt, the saturation of the weak deposits on the steep slope leads to debris flows. These debris flows are deposited in the newly formed sediment trap formed by the fault rupture. Erosion of the scarp may also lead to some deposition in the sediment trap at this time, although evidence to support or deny this possibility was not recognized. After geomorphic stability returns to the slope to the south of the drainage basin, sedimentation

at the trench site is dominated by fine grained slope wash and organics formed in situ. The stratigraphy south of the shear zone is described as 8 packages of soil, generally comprising a lower subunit of coarse sediments with a fine-grained matrix overlain by a subunit of fine-grained material. The packages are numbered from the top downward, and the upper and lower subunits were labeled a and b, respectively. Our interpretation follows that the coarse soil layers are deposited at, or soon after, earthquakes on this fault strand. Paleoseismic investigations at Alayurt (Hartleb et al., 2003) and Destek (Fraser et al., 2009), which are also situated on the 1943 rupture segment, also recognized increased coarse allochthonous sediments above event horizons overlain by more autochthonous sediments. The best test of this interpretation is to compare the timing of earthquakes derived in this study to the pre-existing earthquake records.

Event Chronology

Because the coarse layers are deposited at or soon after earthquake events, the base of these layers are considered to be event horizons. The trench revealed the base of 7 coarse sediment layers which constitute event horizons. The age of these 7 event horizons constrain the age of 7 earthquake events. Of the 170 charcoal samples collected from the trench, 31 charcoal samples have been radiocarbon dated (Table. 1). To accurately constrain the timing of earthquakes an ordering-constrained Bayesian model was constructed using OxCal (Bronk Ramsey, 2007), a program which also calibrates the radiocarbon ages into calendar ages. Firstly, an unconstrained OxCal model (calibrated dates in stratigraphic order, but not grouped in a sequence) was constructed to evaluate and exclude sample ages which contradict their stratigraphic positions (Electronic supplement 3). In sediment packages 1 to 6, samples 46, 147, and 149, are excluded as they are interpreted as reworked. Reworking is not surprising as the sediments are predominantly sourced from the drainage basin south of the trench site which can function as storage for charcoal. In packages 7 and 8 the dating results are less conformable. A conservative approach was taken and samples 163, 165 and 167 were excluded because they appear to be reworked, and samples 91 and 134 were excluded because they are too young, which is attributed to contamination of these deposits by younger carbon. Contaminant samples are derived from younger charcoal transported into the subsurface, by being washed into a soil macro-pore, or by bioturbation (i.e.

moles, worms, tree root deformation). Sample 113b is not used in the model because it is comprised of the base-soluble fraction of sample 113. The base-soluble fraction is composed of smaller organic molecules that are attributed to degradation of the original organic molecules and contamination by mobile organic molecules. Sample 113a is composed of the base-insoluble fraction that is composed of the original intact molecules. Samples 113a and 113b provided similar ages which indicates that there is only a small amount of chemical degradation or contamination of the charcoal samples in this trench after deposition. In the second phase, a constrained OxCal model was compiled using the remaining 23 radiocarbon ages (Fig. 5a) to accurately determine the precision and timing of 7 earthquakes (Table. 2) and the duration between them (Fig. 5b, Table. 3). In this model, samples from individual subunits were grouped into "phases" (relative-order unspecified), and these phases were grouped into a sequence according to their stratigraphic order. We used boundaries with uninformative priors at the start and end of the sequence. For each inferred event horizon, an empty "Date" statement was inserted between the bounding subunits/phases.

The event horizon at the base of package 1 (i.e. between units 1b and 2a) corresponds to event 1 and the event horizon at the base of package 2 corresponds to event 2, etcetera. Interestingly, event 1, which occurred between 549 AD and 651 AD (incorporating the 2σ uncertainty), is far too old to be the 1943 Tosya Earthquake, which indicates that this earthquake record is relict i.e. it does not extend to the present. There are three additional independent lines of evidence which indicate that active sedimentation ceased at the trench site a considerable time ago. Firstly, a large zone of deformation and alteration on the upper east wall is attributed to a tree root. This zone extends to the surface which indicates that a tree grew at the present ground surface. The tree would have taken some time to grow and presently there is no evidence of this tree at the surface or any significant tree material in the trench, so it must have died a considerable time ago. Secondly, the shear zone in the trench is very well developed and extends right to the base of the plough zone. Several events must have occurred to develop this highly sheared zone to near the surface. If sedimentation had continued to the present we would expect to see a general decrease in deformation towards the surface, possibly including

some upward fault terminations. Thirdly, the evolution of the local hydrologic system provides a clear sequence of events which explains why this site has been relict.

Figure 6 graphically shows our interpretation of the local geomorphic evolution. At first, prior to incision of the XX stream and the YY channel, there is an alluvial fan formed by the XX stream and some other local streams (Fig. 6a). Then an earthquake caused offset of the alluvial fan, forming a small upslope-facing scarp (Fig. 6b). The upslope-facing scarp formed a sediment trap which caught cyclic sedimentation from the steep slope south of the trench site (Fig. 6c). Fan offset (Fig. 6b) and deposition of sediments (Fig. 6c) occurred at least eight times, which gives us the earthquake record exposed in the trench. Furthermore, this process explains the formation of the side-hill bench at this location. Around 1000AD the XX stream began to incise into the alluvial fan surface, locking the stream in its course. Water flowing from the steep slope south of the trench site started to drain into XX stream and within a short period of time the YY channel had formed (Fig 6d). The YY channel isolated the sediment trap from the sediment supply until the present.

Because the small drainage basin (2.1 ha) of the YY channel, formerly a steep slope to the south of the trenched side-hill bench, is unlikely to have enough water flow to mobilize cobble-sized clasts, the coarser layers probably reflect debris flow deposits while the fine-grained materials are alluvial (slope wash) deposits from rainfall events. This is consistent with the mixed, usually matrix-supported nature of the coarse layers. Prior to incision of the YY channel, bed load and debris flows were deposited on the side-hill bench due to the lower gradient. After incision of the YY channel, sediments were transported into the XX steam because the stream and debris flows are channelized. It is inferred that this small channel was incised around the time the XX stream incision began.

A small channel form incised into the side-hill bench adjacent to the XX stream is interpreted to have formed at the initial stage of incision and to have been subsequently abandoned. A small pit was opened in this channel form to expose the underlying fan gravels, and a charcoal sample (Surface sample) was collected from below the top soil and above the gravel at a depth of approximately 40 cm. The surface sample yielded an age very similar to the age of the samples in unit 1b at the top of the trench strata

(Table 1, Fig. 5). This strongly links the timing of the end of sedimentation on the side-hill bench with stream incision. Following the incision of the XX stream several earthquakes have occurred and this is evidenced by the right-lateral offset of the XX stream by 23.5±1.5 m (Fig 6e).

Discussion

Comparison to existing studies

To both validate this study and consider the mechanics of the NAF, a comparison is drawn between the results of this study, other paleoseismic studies on the 1943 rupture segment, and the historical record. This is made a little more difficult because the record is relict. To ensure that appropriate comparisons are drawn, the studies from Havza (Yoshioka et al., 2000) and Alayurt (Hartleb et al., 2003) are reinterpreted using OxCal (Bronk Ramsey, 2007) order-constrained models. This ensures comparison of results is not biased by variable procedures of interpretation. The study from Destek (Fraser et al., 2009) already uses an OxCal model so we use their results. The investigation at Ilgaz (Sugai et al., 1999) does not provide adequate data to allow a re-interpretation, therefore we present their conclusions in the original form (Fig. 7). Figure 7 compares the event probability distribution functions (PDFs) determined from studies on the 1943 Tosya Earthquake rupture segment with the historical event which we considered may correlate to earthquakes on this segment. The PDFs are labeled from the top down using the first letter of the site name. All of the other studies in this segment identified evidence of the 1943 Tosya earthquake.

Hartleb et al (2003) conducted a detailed trench study of a sag pond at Alayurt. Their study constrained the timing of 6 earthquakes including the Tosya earthquake (their event 1). They present the conventional radio carbon ages ("measured radiocarbon age") which we used to make an OxCal model. Hartleb et al (2003) presented 2 possible scenarios associated with the antepenultimate event at Alayurt based on uncertainty of whether the samples above the event horizon are reworked or not. Both scenarios are plotted as A2a and A2b in Figure 7. For the 5th event identified at Alayurt (A4 Fig. 7) Hartleb et al (2003) considered sample 120 to be reworked, therefore we also did not use sample 112 which has a similar age. We do not include the dates associated with a sixth event in the

4^{th} or 5^{th} millennium BC identified by Hartleb et al (2003) in our model because this is not useful for comparison with other data.

Near Havza, Yoshioka et al (2000) undertook an investigation that they interpreted to reveal the timing of 3 earthquakes including the Tosya earthquake. We agree with the event horizons that Yoshioka et al (2000) interpreted, but we recognize an additional event horizon based on fault terminations. In Figure 4 of Yoshioka et al (2000), which is the log of the east wall of the trench, the additional event horizon is on the north side of the fault where a poorly defined gravel layer rests on a fault termination at grid location horizontal 2 vertical 7. In Figure 5 of Yoshioka et al (2000), which is the log of the west wall of the trench, (NB: we assume that the indication of north and south on this figure is accidentally reversed) we recognise the additional event horizon below a gravel layer with a distinct channel form. This is evidenced by a fault termination at approximately horizontal 1, vertical 2 and other fault terminations near the base of this sand and gravel unit.

Relative to other paleoseismic investigations on the 1943 rupture segment it is evident that the 3 most recent earthquakes are absent from the earthquake record determined in this study (Fig. 7a). The first event identified in this study (E1) correlates to identified at Ilgaz (Sugai et al., 1999), Havza (H2) (Yoshioka et al., 2000), Alayurt (A3) (Hartleb et al., 2003), and particulaly well to Destek (D3) (Fraser et al., 2009) (Fig. 7b). This event may correlate to the historical 529 AD earthquake (Guidoboni et al., 1994). Notably, the 2σ (95.4%) age range for this event, 549 – 641 AD, does not overlap with the 529 AD earthquake (Fig. 7), however the 3σ (99.7%) age range of for this event is 458 – 662 AD. Furthermore, the PDFs for the same event at Alayurt (A3) and Destek (D3) also have most of their probability after the 529 AD earthquake.

The historical earthquake in 235/236 AD reported at Amasya (Guidoboni et al., 1994) only correlates with event D4 identified at Destek which Fraser et al. (2009) interpreted as being up to three separate events. At Alayurt, Hartleb et al. (2003) interpreted the event that we have called A4 as being caused by this earthquake, however our reanalysis suggests that this is not likely. The limited extent of historical reports for this event corroborates the fact that this event is only identified at Destek. This suggests that the eastern end of the 1943 rupture segment (S1 in Fig. 1c) sometimes ruptures

independently or with adjacent segments to the east. Perhaps the Ladik L. releasing step-over, which has a step-over-distance of ~1 km (Barka and Kadinsky-Cade, 1988), occasionally behaves as a barrier to fault rupture.

Event E2 (Fig. 7) correlates to event I4 identified at Ilgaz (Sugai et al., 1999), possibly to the poorly constrained event A4 at Alayurt (Hartleb et al., 2003), and to event D5 from Destek (Fraser et al., 2009) assuming that D4 does correlate to the 235/236 AD earthquake. Event E2 does not correlate to any event envelopes determined at Havza (Yoshioka et al., 2000). This event may be missing from the earthquake record at Havza (Yoshioka et al., 2000) or possibly event A4 from Alayurt (Hartleb et al., 2003) correlates to an older earthquake and segment S2 did not rupture while segments S1 and S3 ruptured as part of two separate earthquakes (Fig. 1c). This event correlates to a cluster of earthquakes reported from near the eastern end of the Marmara Sea in 29 AD (Guidoboni et al., 1994), 32 AD (Ambraseys, 2002; Ambraseys and Jackson, 1998), 68 AD (Ambraseys, 2002), and 69 AD (Guidoboni et al., 1994) (NB. these events may be 2 events reported with different dates by different authors).

Event E3 (Fig. 7) has a broad temporal envelope and may correlate to event D6 from Destek (Fraser et al., 2009) and possibly event A4 from Alayurt (Hartleb et al., 2003). There is no mention of this event in historical earthquake record literature probably because the historical record is far from complete before 0 AD. Event E4 (Fig. 7) identified in this study correlates with event D7 from Destek (Fraser et al., 2009), and possibly event A4 from Alayurt (Hartleb et al., 2003), in the oldest quarter of the first millennium BC. Event E5 (Fig. 7) occurred at 1227 – 968 BC, which may possibly correlate to event A4 from Alayurt (Hartleb et al., 2003), is consistent with the proposed earthquake that caused the destruction of the ancient cities of Hattusas, Karaoglan, and Alca Hoyuk (amongst others) ~1200 BC (Nur and Burgess, 2008; Nur and Cline, 2000). This observation supports the idea that the end of the Bronze Age in the Aegean and Eastern Mediterranean Region was associated with at least 1 large earthquake on the NAF and possibly a seismic cycle. Event E6 is comparable to event H3 identified at Havza (Yoshioka et al., 2000). Event E7 (Fig. 7, Table 2) is not comparable to any existing earthquake records.

Our reanalysis of the other studies on the 1943 rupture segment shed some light on the earthquake record over the last millennium. We attribute the PDFs I1, A1, and D1 from Ilgaz, Alayurt, and Destek, respectively, to either of the historical earthquakes which occurred in 1668 AD or 1598 AD. The PDF of event A1, from Alayurt, suggests that the 1598 AD earthquake is a better fit, however the extent of damage caused in Ankara and other cities suggests that the 1668 AD earthquake(s) was larger and therefore more likely to have ruptured this segment of the fault. Event PDFs H1, A2a, and D2 suggest there was an earthquake on segments S1 and S2 sometime between 1200 AD and 1400 AD, although there are no historical records to support this inference. However, event PDFs I2, A2b, and weakly D2 corroborate historical earthquakes in either 1035 AD or 1050 AD. Therefore, we are unable so say which of the 2 scenarios proposed for event A2 at Alayurt is more probable.

It is important to remember that the PDFs generated in this, and other paleoseismic investigations, describe only the error associated with determining the age of samples (i.e. laboratory and calibration error). Other sources of error that are not quantified include; 1) error associated with interpreting the history of samples prior to deposition, 2) interpretation of the stratigraphy, and 3) the locations of the samples relative to the event horizon (this can be used in cases where a constant sedimentation rate is assumed i.e. lakes and peat soils). Therefore, the PDFs established in this study may not incorporate the actual timing of earthquakes. Furthermore, the absence of evidence for surface rupture in some trenches over some time periods is not evidence that earthquakes did not rupture that section of the fault.

Validation of our interpretation that earthquakes caused the deposition of coarse sediment layers in the trench stratigraphy is made difficult because the record is relict. However, events 1 and 2 identified by this study are comparable to the results from other studies on the 1943 rupture segment of the NAF. Additionally, the event E5 is consistent with a proposed earthquake sequence around 1200 BC. Therefore, we infer that the earthquake record in this study is reliable and probably complete from the 529 AD earthquake until the early third millennium BC. To be sure of this interpretation more paleoseismic data concerning these events are desirable for comparison.

Recurrence interval

Table 3 shows the 2σ age range of the six inter-event times (IETs) between the seven earthquakes identified in this study, the data is also shown graphically in Figure 5b. The recurrence interval can be determined in 2 ways: 1) by dividing duration between the youngest and oldest events, by the number of cycles (the number of events minus 1), or 2) by summing the interval PDF's that can be determined between each successive event. The first method yields an average recurrence interval, which does not take into account possible variability of inter-event times, but is also not influenced by uncertainties on the dates of the intervening events. The recurrence interval is 471 – 529 years (2σ). The second method incorporates both uncertainties on the dates of each event, and the natural variability of inter-event times. The summed inter-event time (SIET) gives a more realistic estimate of the time between earthquakes locally of 97 – 912 years. This estimate is consistent with the findings of other studies on the NAF, for example 280 – 620 years at Ilgaz (Sugai et al., 1999), 250 – 800 years at Alayurt (Hartleb et al., 2003), 61 – 690 years at Destek (Fraser et al., 2009), and a less certain estimate of 600 – 900 years from Havza (Yoshioka et al., 2000).

Slip-rate

Based on the 23.5±1.5 m (Fig. 3d) offset of XX stream, a horizontal, fault parallel, slip-rate is estimated (Fig. 8). The 1.5 m error of the offset accounts for 2 standard deviations of the displacement estimated by calculating the offset in a range of different ways. Notably, the offset is determined parallel to the general trend of the fault locally (~E – W), not the immediate principal strand, to ensure a slip-rate relevant to the local trend of the fault. The age of the surface sample and the samples near the top of the trench indicate that the 529 AD earthquake occurred before stream incision and the offset probably did not begin until the subsequent earthquake, which probably occurred early in the eleventh century (1035 or 1050 AD) (Fig. 8). To calculate the slip-rate the pre 1943 Tosya earthquake stream displacement is divided by the period between the 1050 AD and 1943 AD earthquakes, taking into account the associated errors. If the post-1943 displacement was included then there would be one more earthquake displacement than seismic cycles, yielding an overestimate of the slip-rate. The displacement of the XX stream prior to the 1943 Tosya Earthquake is estimated as 21±1.9 m using the 23.5±1.5 m present offset minus 1.6 – 2.4 m offset measured at Kamil after the last event (Barka,

1996). Therefore, the local horizontal slip-rate, over the last thousand years at Elmacik, is about 21.4 – 25.6 mm/yr. This estimate of slip-rate is consistent with estimates of slip-rate from GPS and other short-term slip-rates on the 1943 rupture segment. Notably, studies which determine offsets over a longer time period estimate lower slip-rates. For example, at Tahtokopru (Kozaci et al., 2009) a preferred slip-rate of 18.6 +3.5/-3.3 mm/yr was determined over the last ~3 ka, which overlaps with the slip-rate from this study around 22 mm/yr. The possible ranges of slip-rates between 1 ka and 3 ka BP is ~10 – 22 mm/yr, derived by dividing the difference in offsets measured at Elmacik and Tahtokopru by 2 ka. The ~3 ka slip-rate from Tahtokopru does not overlap with the GPS slip-rate of 24.5 ± 1.5 mm/yr. This suggests that the rate of displacement is about 22 mm/yr and the GPS slip-rate is wrong, or that plate movement has been accelerating over the last few thousand years. Changes in rates of motion may reflect a recent increase in the rate of deformation in the lower crust (Kozaci et al., 2009) although short sampling periods of fault displacement rates on normal and reverse fault systems have been shown to be unreliable (Mouslopoulou et al., 2009).

GPS data modeled with an elastic Anatolian plate suggest that there is a significant component of fault-normal extension occurring on this section of the fault (Flerit et al., 2004). While we can not make a reliable estimate of this from our study about 4.5 m of vertical, down to the south, displacement is recognized in the trench strata relative to the height of the weathered scarp. If it is assumed that all of this displacement is caused by regional displacement rather than local transpression or transtension, then using the approximate age of the oldest event in the trench (4500 yrs) a vertical slip-rate of ~1 mm/yr is estimated.

Displacement per event

Because 23.5±1.5 m (Fig. 3d) offset of XX stream appears to have been caused by three earthquakes, the 1.4 m to 2.6 m of right-lateral displacement caused by the 1943 Tosya earthquake recognized near Kamil (Barka, 1996) suggests that the offsets during the two preceding earthquakes had an average right-lateral offset in the order of 10 m (Fig. 8). This relationship was also observed in the Eksik basin (Kozaci et al., 2007). However, an offset of 45 – 65 m was measured at Tahtokopru over the last ~3000 years (Kozaci et al., 2009) and over that period 8 or 9 earthquakes are recorded in our trench (including the

1943 Tosya earthquake) yielding a long term average displacement per event of 5 – 7.2 m. Therefore the 1943 Tosya earthquake caused an anomalously small displacement, whereas the preceding two earthquakes, in 1668 and the eleventh century, had anomalously large average displacements per event.

Assuming a slip-rate of 22 mm/yr, the summed inter-event time of 97 – 912 years corresponds to accumulated slip deficit of ~2 – 20 m. The local measurements of the displacements associated with the Tosya earthquake indicate that this event was very much at the smaller end of the range of earthquake magnitudes that rupture this segment of the fault. It also indicates that the Tosya Earthquake released less than ~100 years of accumulated stress. This may reflect the large stress drop associated with the two preceding earthquakes, or a stress drop deficit which raises the risk of the next earthquake locally.

Conclusions

A paleoseismic trench situated on an incised side-hill bench formed by an upslope-facing fault scarp has revealed the timing of a relict series of surface-rupturing earthquakes in the central portion of the, 280km long, 1943 Tosya earthquake rupture segment of the North Anatolian Fault. The XX stream, which is situated next to the trench site, incised into the local topography around 1000 years ago. This stream incision caused a small channel (YY channel) to form across the side-hill bench on which the trench site was located. The YY channel rerouted sediments derived from a steep slope south of the side-hill bench that were previously deposited on the side-hill bench. The paleoseismic trench excavated across a rounded fault scarp on the side-hill bench revealed 8 sedimentary packages, each comprising a coarse-grained unit overlain by a fine-grained unit, juxtaposed against a deformed alluvial gravel deposit. Prior to the incision of the YY channel, earthquakes caused increased erosion of coarse material from the adjacent steep slope, which were deposited by debris flows onto the side-hill bench due to the lower gradient. Between earthquakes finer-grained deposits formed by slope wash from the steep slope and in situ formation of organics. The base of each coarse unit is interpreted to be an earthquake event horizon. Using radiocarbon dating the timing of 7 earthquakes is constrained. The youngest event correlates to the historical 529 AD earthquake, which was also identified in the 4 pre-existing paleoseismic investigations on the 1943 rupture

segment. A second event is constrained to about the first century AD which correlates with an event identified in a paleoseismic trench to the west of this study on the 1943 rupture segment. Five further earthquakes are constrained to 609 – 185 BC, 971 – 814 BC, 1227 – 968 BC, 2050 – 1777 BC, and 2556 – 2235 BC. The summed inter-event times of the earthquake record is 97 – 912 years (2σ), and the average recurrence interval is 471 – 529 years (2σ).

The fifth oldest earthquake identified at this site (1227 – 968 BC) corresponds to a sequence of earthquakes proposed based on archaeological information ~1200 BC. This earthquake is only clearly evidenced at Elmacik, which is presumably because other paleoseismic records are incomplete during this period. More widespread earthquake timing information for this period is required to validate this inference over the whole region.

The stream incised next to the trench site has been offset by 23.5±1.5 m since sedimentation stopped in the trench. Using the time and displacement between the 1050 AD and 1943 AD earthquakes the horizontal fault-parallel slip-rate is estimated at 21.4 – 25.6 mm/yr. This overlaps, at 22 mm/yr, with a slip-rate derived over a ~3 ka period at Tahtakopru (Kozaci et al., 2009). However, differences between the ~3 ka and GPS estimates of slip-rate are not reconcilable suggesting that either GPS estimates are wrong, the geological estimates are too crude, or our preferred interpretation is that the slip-rate has been accelerating over the past few thousand years at least.

We determined a long-term displacement per event of 5 – 7.2 m using our earthquake record in conjunction with the historical earthquake record and a ~3 ka displacement measured at Tahtakopru (Kozaci et al., 2009). The 1943 Tosya earthquake only caused 1.4 m to 2.6 m of right-lateral displacement (Barka, 1996) making this event anomalously small. The two earthquakes preceding the 1943 earthquake, probably in 1668 AD and the eleventh century, are inferred to have caused on average more than 10 m of displacement per event, making them anomalously large. It is probable that the 1943 event only accommodated ~100 years of stress accumulation. Therefore this segment of the fault may well still have a considerable amount of accumulated stress. However, lower slip-rates determined over longer periods of time on this section of the NAF suggest that the long-term rate of deformation is lower than that of the last two millennia, suggesting that

the inter-event time estimated over long periods of time may not be applicable to the future.

Studying a sedimentary sequence to constrain the timing of earthquakes differs from most paleoseismic studies which rely on structural relationships. This technique is in essence similar to identifying earthquakes in other sedimentary records such as lake sediments. The surface ruptures and ground shaking caused by earthquakes cause extensive erosion especially in steep terrain. Because of the simple relationship between drainage basin response to earthquakes, and the sedimentary record of the drainage basins, long earthquake records can be deduced allowing interrogation of the relationships between fault rupture at different sites over long periods of time.

8.0 Acknowledgements

Our field studies were greatly enhanced by the organizing assistance of Dr. Erhan Altunnel from Osmangazi University, Eskishir, Turkey. Thanks to; Dr Arif Gonulol and Ondokuz Mayis Universitesi for assistance with logistics, Jeff Pigati and Jim Willson from Aeon Laboratories for remarkable turn around times on radiocarbon dating. We acknowledge the European Commission for funding this project as part of the Marie Curie Excellence Grant Project "Understanding the irregularity of seismic cycles: A case study in Turkey" (MEXT-CT-2005-025617: Seismic Cycles).

9.0 References

Ambraseys, N., 2002, The Seismic Activity of the Marmara Sea Region over the Last 2000 Years: Bulletin of the Seismological Society of America, v. 92, p. 1-18.

Ambraseys, N.N., 2001, Reassessment of earthquakes, 1900-1999, in the Eastern Mediterranean and the Middle East: Geophysical Journal International, v. 145, p. 471-485.

Ambraseys, N.N., and Finkel, C., 1995, The Seismicity of Turkey and Adjacent Areas: A Historical Review, 1500-1800: Istanbul, Muhittin Salih Eren.

Ambraseys, N.N., and Finkel, C.F., 1987, Seismicity of Turkey and neighbouring regions, 1899-1915: Annales geophysicae. Series B. Terrestrial and planetary physics, v. 5, p. 701-725.

Ambraseys, N.N., and Jackson, J., 1998, Faulting associated with historical and recent earthquakes in the Eastern Mediterranean region: Geophysical Journal International, v. 133, p. 390-406.

Barka, A., 1996, Slip distribution along the North Anatolian fault associated with the large earthquakes of the period 1939 to 1967: Bulletin of the Seismological Society of America, v. 86, p. 1238-1254.

Barka, A.A., 1992, The North Anatolian fault zone: Annales Tectonicae, v. 6, p. 164–195.

Barka, A.A., Akyüz, S.H., Cohen, H.A., and Watchorn, F., 2000, Tectonic evolution of the Niksar and Tasova-Erbaa pull-apart basins, North Anatolian Fault Zone: their significance for the motion of the Anatolian block: Tectonophysics, v. 322.

Barka, A.A., and Hancock, P.L., 1984, Neotectonic deformation patterns in the convex-northwards arc of the North Anatolian fault zone, The Geological Evolution of the Eastern Mediterranean. Geological Society of London, Special Publications, Volume 17, p. 763–774.

Barka, A.A., and Kadinsky-Cade, K., 1988, Strike-slip fault geometry in Turkey and its influence on earthquake activity: Tectonics, v. 7, p. 663-684.

Bronk Ramsey, C., 2007, OxCal version 4.0.5 Radiocarbon Calibration software.

Drews, R., 1993, The end of the Bronze Age: changes in warfare and the catastrophe ca. 1200 BC, Princeton University Press.

Flerit, F., Armijo, R., King, G., and Meyer, B., 2004, The mechanical interaction between the propagating North Anatolian Fault and the back-arc extension in the Aegean: Earth and Planetary Science Letters, v. 224, p. 347-362.

Fraser, J.G., Pigati, J.S., Hubert-Ferrari, A., Vanneste, K., Avsar, U., and Altinok, S., 2009, A 3000-year record of ground-rupturing earthquakes along the central North Anatolian Fault near Lake Ladik, Turkey: Bulletin of the Seismological Society of America, v.?, p.?

Guidoboni, E., and Comastri, A., 2005, Catalogue of earthquakes and tsunamis in the mediterranean area from the 11th to the 15th century: Bologna, Istituto Nazionale de Geophysical e Vulcanologia.

Guidoboni, E., Comastri, A., and Traina, G., 1994, Catalogue of ancient earthquakes in the Mediterranean area up to the 10th century, Istituto nazionale di geofisica, 504 p.

Hartleb, R., Dolan, J., Akyüz, H., and s Yerli, B., 2003, A 2000-Year-Long Paleoseismologic Record of Earthquakes along the Central North Anatolian Fault, from Trenches at Alayurt, Turkey: Bulletin of the Seismological Society of America, v. 93, p. 1935-1954.

Hubert-Ferrari, A., Armijo, R., King, G., Meyer, B., and Barka, A., 2002, Morphology, displacement, and slip rates along the North Anatolian Fault, Turkey: J. Geophys. Res, v. 107, p. 2235.

Keefer, D.K., and Moseley, M.E., 2004, Southern Peru desert shattered by the great 2001 earthquake: Implications for paleoseismic and paleo-El Nino-Southern Oscillation records: Proceedings of the National Academy of Sciences, v. 101, p. 10878-10883.

Kozaci, O., Dolan, J.F., Finkel, C.F., and Hartleb, R., 2007, Late Holocene slip rate for the North Anatolian fault, Turkey, from cosmogenic 36Cl geochronology: Implications for the constancy of fault loading and strain release rates: Geology, v. 35, p. 867-870.

Kozaci, O., Dolan, J.F., and Finkel, R.C., 2009, A late Holocene slip rate for the central North Anatolian fault, at Tahtakopru, Turkey, from cosmogenic ^{10}BE geochronology: Implications for fault loading and strain release rates: Journal of Geophysical Research, v. 114, p. B01405.

Lettis, W., Bachhuber, J., Witter, R., Brankman, C., Randolph, C.E., Barka, A., Page, W.D., and Kaya, A., 2002, Influence of Releasing Step-Overs on Surface Fault Rupture and Fault Segmentation: Examples from the 17 August 1999 Izmit Earthquake on the North Anatolian Fault, Turkey: Bulletin of the Seismological Society of America, v. 92, p. 19-42.

Matthews, R., 2009, Chapter Five: A Dark Age, Grey Ware and Elusive Empires: Paphlagonia through the Iron Age, 1200-330 BC, *in* Matthews, R., and Glatz, C., eds., At Empires' Edge: Project Paphlagonia. Regional Survey in North-Central Turkey, Volume Monograph 44: London, British Institute at Ankara.

Mouslopoulou, V., Walsh, J.J., and Nicol, A., 2009, Fault displacement rates on a range of timescales: Earth and Planetary Science Letters, v. 278, p. 186-197.

Nur, A., and Burgess, D., 2008, Apocalypse: earthquakes, archaeology, and the wrath of God, Princeton University Press, 309 p.

Nur, A., and Cline, E.H., 2000, Poseidon's horses: Plate tectonics and earthquake storms in the Late Bronze Age Aegean and Eastern Mediterranean: Journal of Archaeological Science, v. 27, p. 43-63.

Pondard, N., Armijo, R., King, G.C.P., Meyer, B., and Flerit, F., 2007, Fault interactions in the Sea of Marmara pull-apart (North Anatolian Fault): earthquake clustering and propagating earthquake sequences: Geophysical Journal International, v. 171, p. 1185-1197.

Reilinger, R., McClusky, S., Vernant, P., Lawrence, S., Ergintav, S., Cakmak, R., Ozener, H., Kadirov, F., Guliev, I., Stepanyan, R., Nadariya, M., Hahubia, G., Mahmoud, S., Sakr, K., ArRajehi, A., Paradissis, D., Al-Aydrus, A., Prilepin, M., Guseva, T., Evren, E., Dmitrotsa, A., Filikov, S.V., Gomez, F., Al-Ghazzi, R., and Karam, G., 2006, GPS constraints on continental deformation in the Africa-Arabia-Eurasia continental collision zone and implications for the dynamics of plate interactions: Journal of Geophysical Research, v. 111, p. 1-26.

Sengor, A., Tuysuz, O., mren, C., Saknc, M., Eyidoan, H., Gorur, N., Le Pichon, X., and Rangin, C., 2005, The North Anatolian Fault: A New Look: Annual Review of Earth and Planetary Sciences, v. 33, p. 37-112.

Stein, R.S., Barka, A.A., and Dieterich, J.H., 1997, Progressive failure on the North Anatolian fault since 1939 by earthquake stress triggering: Geophys. J. Int, v. 128, p. 594–604.

Sugai, T., Emre, O., Duman, T., Yoshioka, T., and Kuscu, I., 1999, Geologic evidence for five large earthquakes on the north Anatolian Fault at Ilgaz, during the last 2000 years -- a result of GSJ - MTA international cooperative research--, *in* Satake, K., and Schwartz, D., eds., The Paleoseismology Workshop: Japan, USGS Open-File Report 99-400, p. 66-72.

von Gall, H., 1966, Die paphlagonischen Felsgraber (Istanbuler Mitteilungen Beiheft 1): Tubingen.

Westaway, R., 2003, Kinematics of the Middle East and Eastern Mediterranean Updated: Turkish Journal of Earth Sciences (Turkish J. Earth Sci.), v. 12, p. 5-46.

Yoshioka, T., Okumura, K., Kuscu, I., and Emre, O., 2000, Recent surface faulting of the North Anatolian fault along the 1943 Ladik earthquake ruptures: Bulletin of the Geological Survey of Japan, v. 51, p. 29-36.

10.0 Figure Captions

Figure 1: 1a: Tectonic setting of the North Anatolian Fault showing the historical earthquake fault ruptures of the 20th century. The field area for this study is shown with a large red star. Small crosses show the location of; 1) Hattusas, 2) Karaoglan, 3) Alca Hoyuk, 4) Musat. Topographic data for this image is from the 120m grid SRTM dataset. 1b: Sites of previous paleoseismic investigations along the 1943 AD Tosya earthquake fault rupture are labelled 1 – 4 corresponding to a studies at Ilgaz (Sugai et al., 1999), Havza (Yoshioka et al., 2000), Alayurt (Hartleb et al., 2003), and Destek (Fraser et al., 2009) respectively. The topographic data in this image is 90m grid SRTM data and the location of the principal fault is based on satellite image interpretation and Figure 3d from Barka and Kadinsky-Cade (1988). 1c: Amount of offset in the historical 1943 Tosya earthquake according to Barka (1996 and references therein); the bottom axis, length along the fault, correlates to Figure 1b. Fault segments are noted on the top of the figure based on Barka and Kadinsky-Cade (1988) with the addition of a segment boundary at Kamil.

Figure 2: a) Tectonic geomorphology map of the study area illustrating the location of settlements, active faults, drainages, geomorphic features and test pit locations. This map was compiled from an Ikonos satellite image which is not presented here.

Figure 3: a) Tectonic geomorphology map of the trench site on an Ikonos satellite image. b & c) Annotated oblique photographs of the trench area, taken from the east and south respectively, illustrating the relief of the area. In box c the fault extends between the black arrows. d) Topographic survey data of the offset stream adjacent to the trench site

showing the method used to determine the offset. Topographic lines are spaced 2 m apart vertically and the grey becomes lighter with elevation.

Figure 4: Trench Logs a) East wall trench log. b) Abridged legend, more detailed descriptions of trench units correlating to the symbols in each unit are presented in electronic supplement 2. c) West wall trench log. d) Magnetic-susceptibility data plotted using kriging which corrects for sampling anisotropy; this does not show any useful information.

Figure 5: a) This graph shows the timing of earthquake events and the radiocarbon sample ages used to constrain them. The model is constrained and "I" shaped symbols show how the samples are grouped into phases. Electronic supplement 3 shows an unconstrained model used to exclude dates from this analysis. Solid black probability distribution functions (PFDs) are the earthquake events, medium grey shows the modelled sample PDFs and the light grey shows the original unconstrained (prior) PDFs. Sample names and names of events (earthquakes) are listed on the left side of the figure. The data used to build this model are listed in Table 1 and the 2σ age range of events is listed in Table 2. b) This graph shows the PDFs of the average recurrence interval (RI), summed inter-event time (SIET), and inter-event time (IET) (i.e. IET 1-2 is the inter-event time between events 1 and 2). The 2σ age range of these values are presented in Table 3. These figures are an edited version of the output from software called OxCal (Bronk Ramsey, 2007).

Figure 6: Sequence of events leading to the trenched sediments forming and becoming relict. a) An alluvial fan associated with amongst others, the XX stream. b) The fault offsets the alluvial fan causing an upslope-facing scarp. c) The fault scarp forms a sediment trap (ST) which is filled first by earthquake-related coarse sediments then fine grained sediments. Stages b and c occurred one after another at least 7 times before stage d. d) Stream XX incised into the local landscape at approximately the same time the YY channel incised across the slope above the sediment trap stopping sedimentation in the sediment trap. e) A trench is excavated across the relict sediment trap (black rectangle) to reveal the earthquake record by which time the incised XX stream has been right-laterally offset. The age of the incision is dated with the surface sample (SS) from a degredational channel incised into the side-hill bench during the initial stage of incision (Fig. 6e).

Figure 7: 7a: A comparison of earthquake timing determined by paleoseismic investigations along the 1943 Tosya earthquake rupture segment of the NAF. The horizontal axis is the approximate distance along the 1943 rupture segment for the different sites, but for each site event PDFs are horizontally scaled according to their annual probability (i.e. the area under each curve is 1); the vertical axis is time. All other studies (i.e. not Elmacik) recognized the 1943 earthquake. Earthquake timing at Ilgaz (Sugai et al., 1999) cannot be reinterpreted because the original data was not presented. The timing of earthquakes at Havza (Yoshioka et al., 2000) and Alayurt (Hartleb et al., 2003) is based on our reinterpretation of their data (see text). Data from Destek (Fraser et al., 2009) is presented in the same form as published data. The timing of historic events is annotated down the right side of the figure (see text for references). 7b: A graph comparing the probability distribution for earthquake timing of events equivalent to the youngest event identified at Elmacik. Line labels correlate to 7a.

Figure 8: A graph showing how the slip-rate has been estimated. The offsets of earthquakes prior to the 1943 AD earthquake are unknown. The grey dotted line shows a

possible scenario where the displacement in the 1050 AD and 1680 AD earthquakes are equal therefore, implying an average displacement per event of about 10m.

Electronic supplements

ES 1: a) An example of a table that can be used in the field, with a sample quality and size classification, to ensure adequate sample distribution for obtaining more precise age control on event horizon age. b) Schematic example of event age probability distribution function (PDF) determination using only upper and lower bounding ages. c) Schematic example of the increased event age precision obtained by determining further sample ages at strategic stratigraphic positions because of the prior knowledge that the bounding ages (from example b) are younger or older than the additional sample ages.

The strategy involves first making a table (ES 1a) of all of the units in the trench with a row for upper, middle, and lower thirds of each unit (more partitions could be made where samples are available). When samples are collected their sample number is listed in the appropriate row of the table and followed by 2 symbols, one which describes the quality of the sample, and a second which describes the size of the sample. This strategy serves two purposes; 1) it ensures that good quality datable samples are collected from the middle upper and lower portions of all units efficiently while in the field, and 2) the table makes deciding which samples to date in subsequent phases of dating considerably easier, quicker, and reduces sample handling – a possible source of contamination. This methodology is particularly useful in the context of employing Bayesian statistics on radiocarbon ages to determine the timing of earthquakes. ES 1b relative to ES 1c shows an idealistic example of the benefit having an additional sample between event horizons bounding ages.

ES 2: Annotated plot of unconstrained (i.e. no Bayesian statistic) calibrated radiocarbon ages.

ES 3: Detailed descriptions of soil units exposed in the trench to augment Figure 4.

Figure1

Click here to download Figure: Fig.1_NAFmapcompressed.pdf

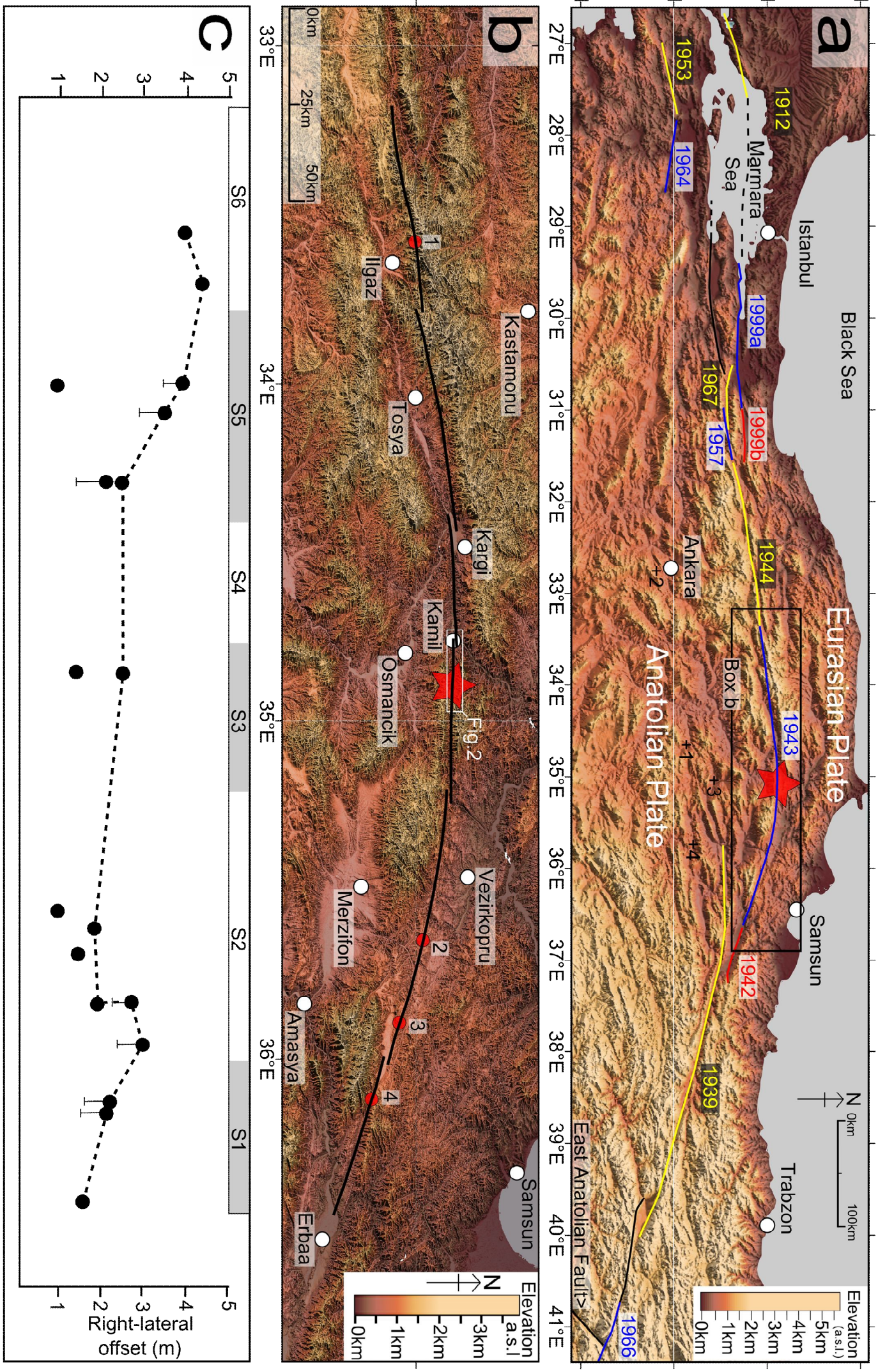

Figure2

Click here to download Figure: Fig.2_Study_area_map.pdf

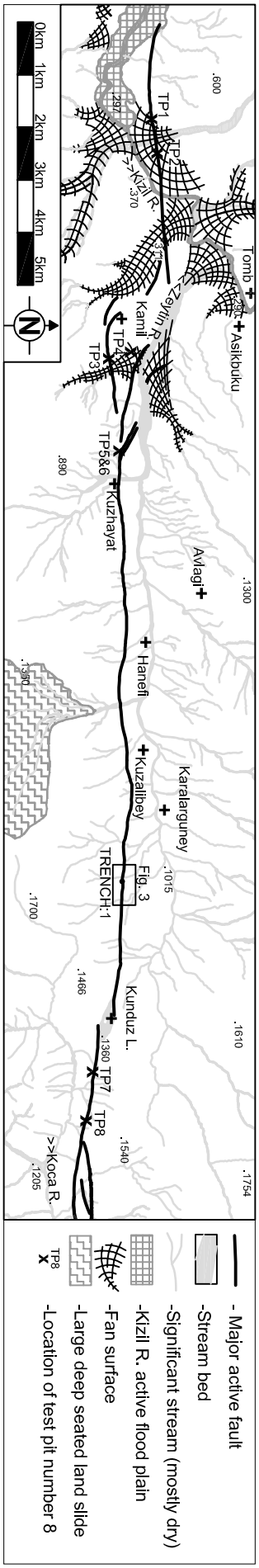

Figure3

Click here to download Figure: Fig.3_SiteMap.pdf

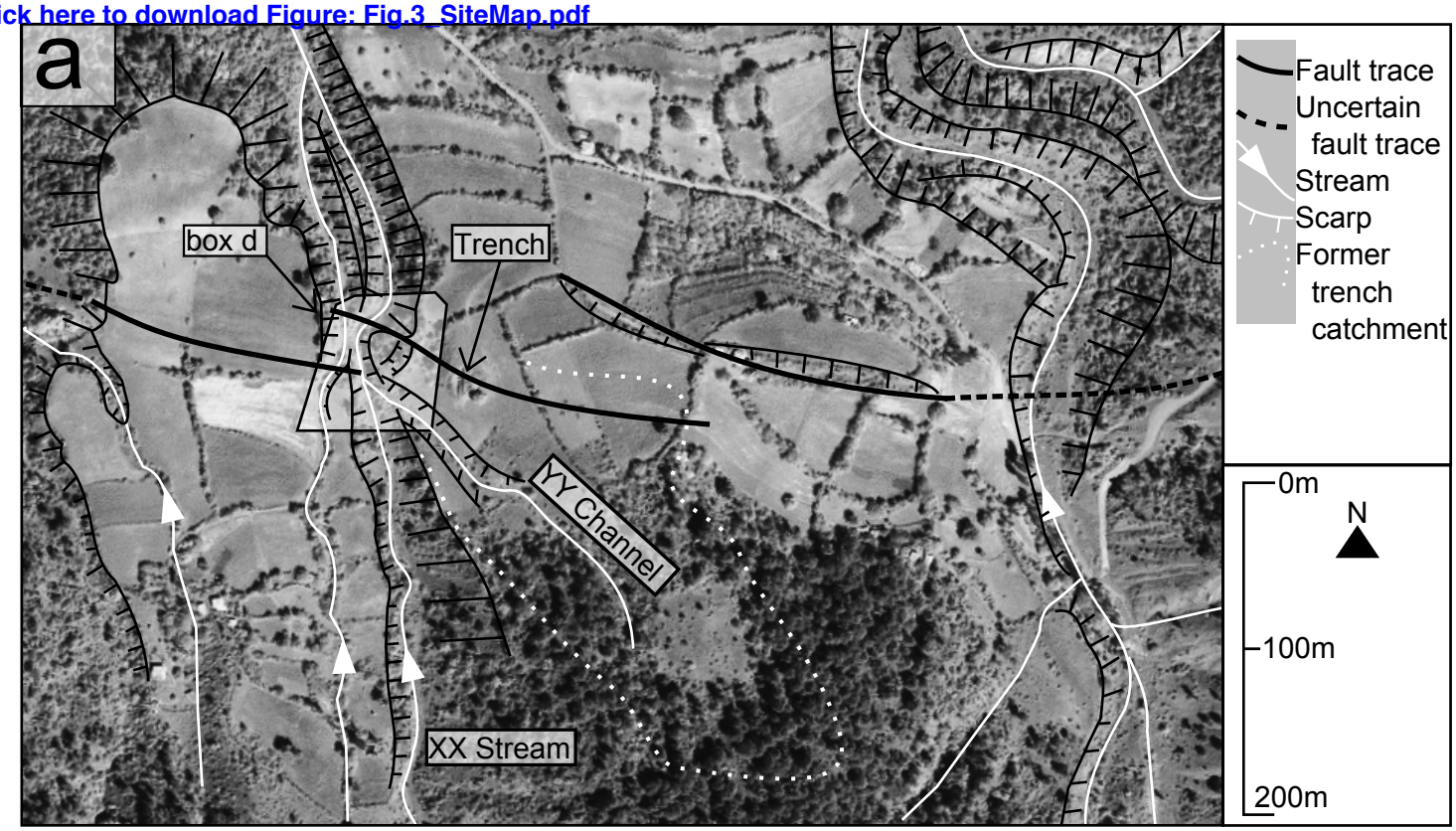

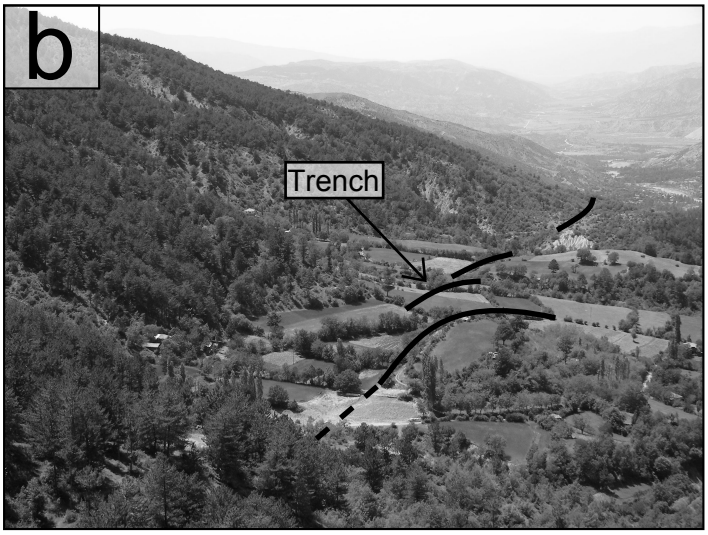

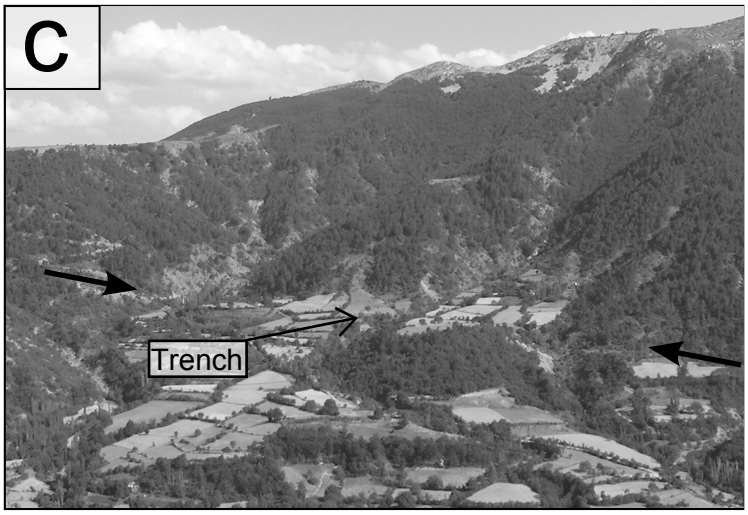

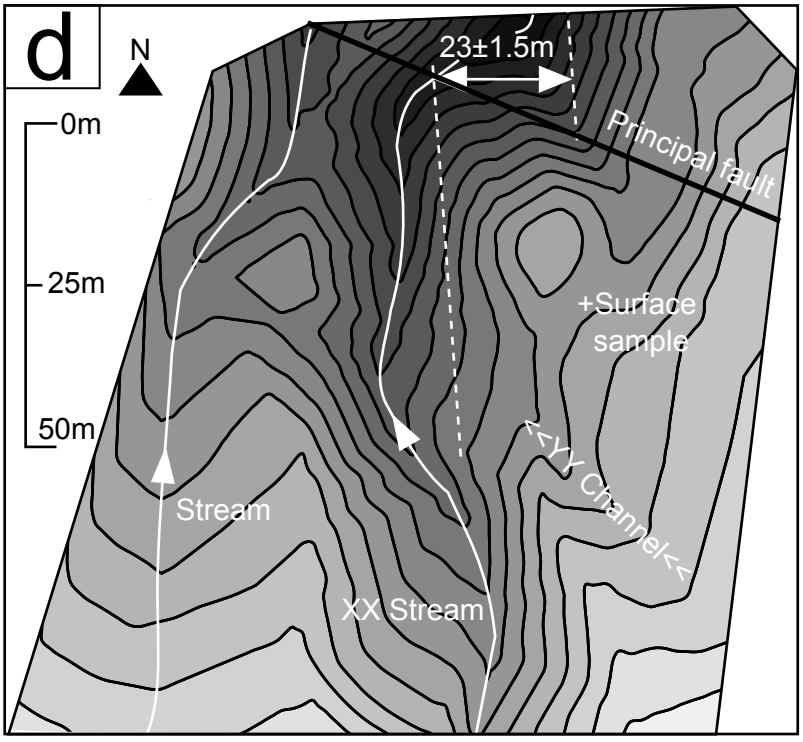

Figure4

Click here to download Figure: Fig.4_TrenchLog.pdf

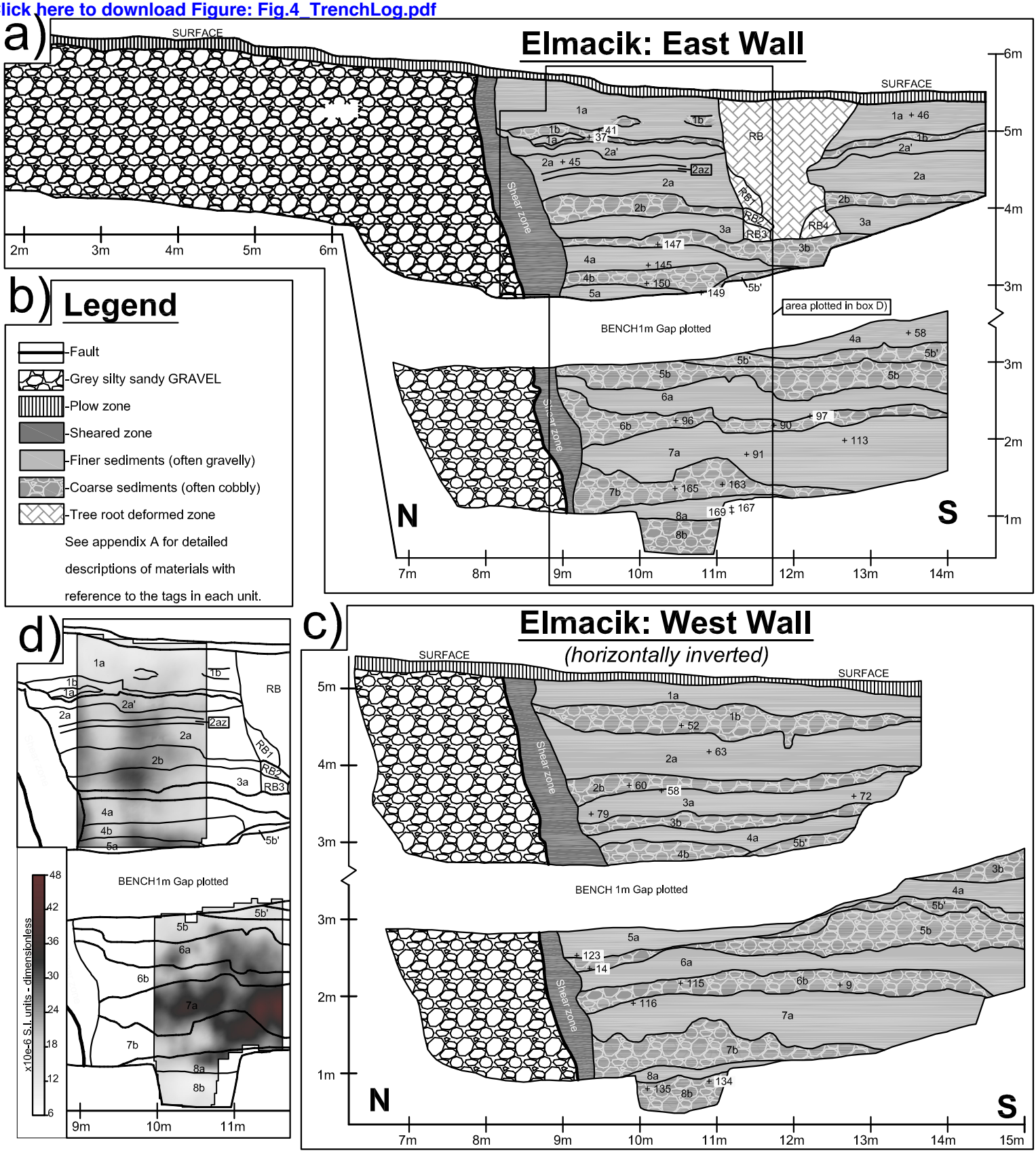

Figure5
Click here to download Figure: Fig.5_Dating.pdf

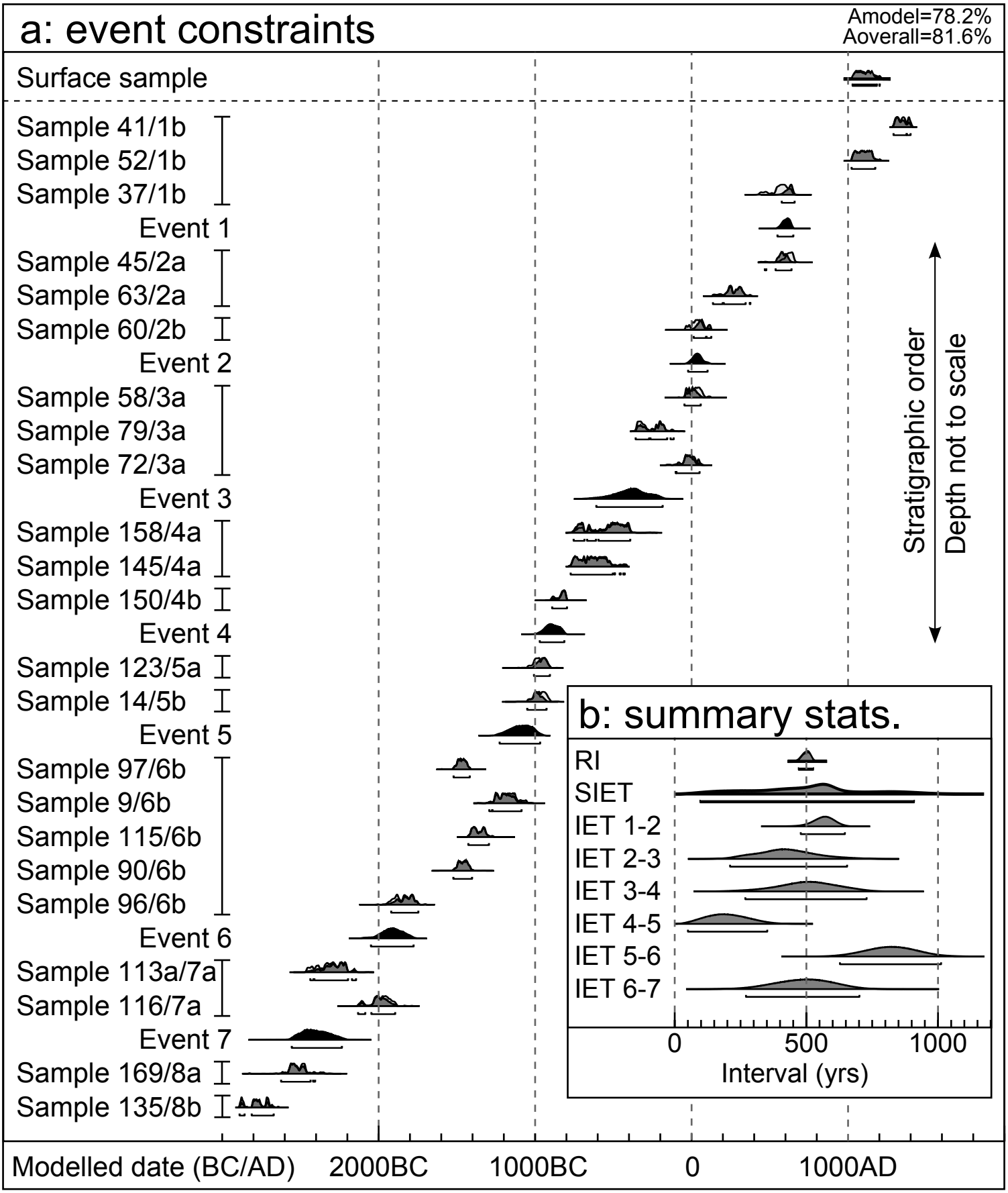

Figure6

Click here to download Figure: Fig.6_SEQ_o_Evts.pdf

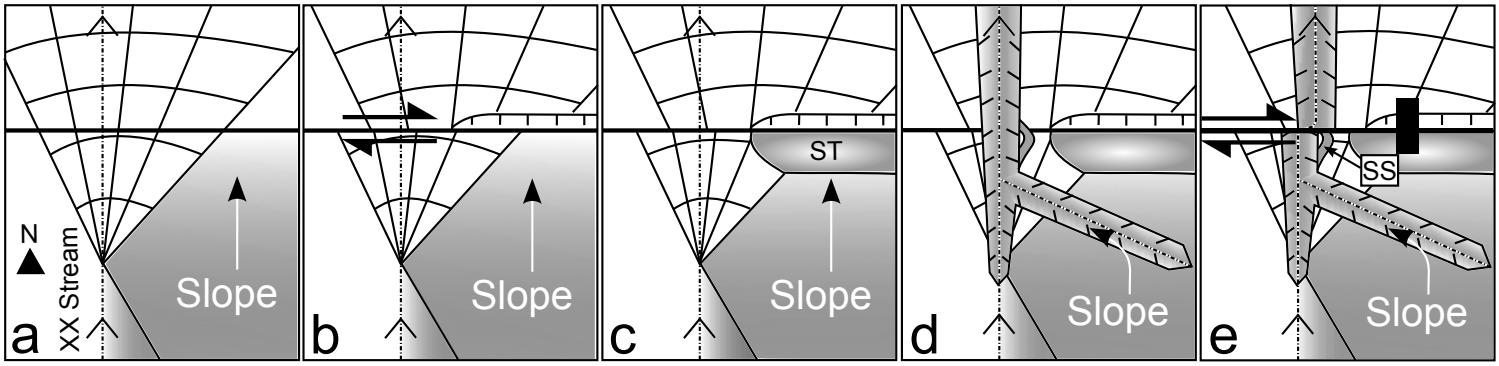

Figure7

Click here to download Figure: Fig.7_EQcompare.pdf

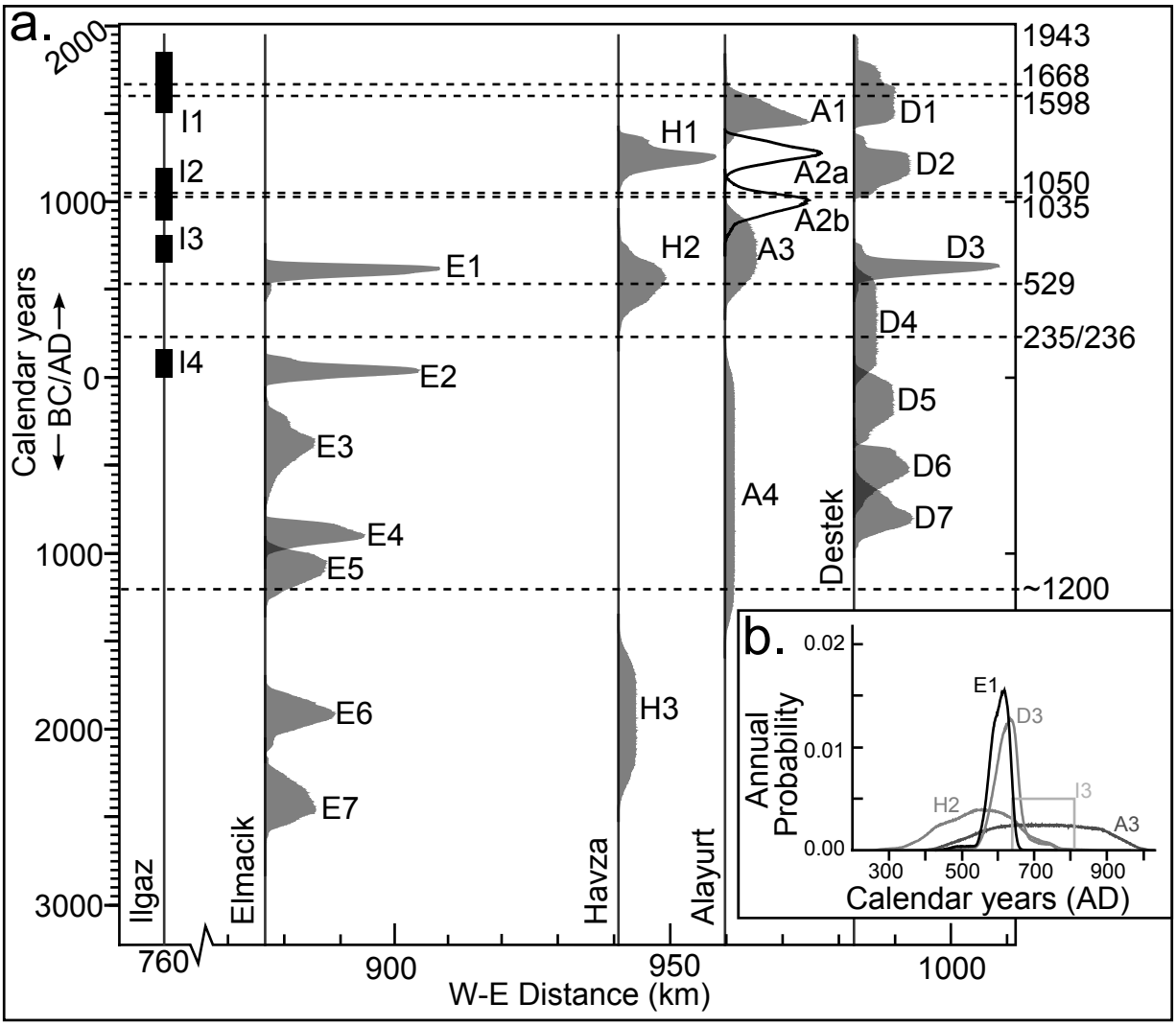

Figure8

Click here to download Figure: Fig.8_S_R_calc.pdf

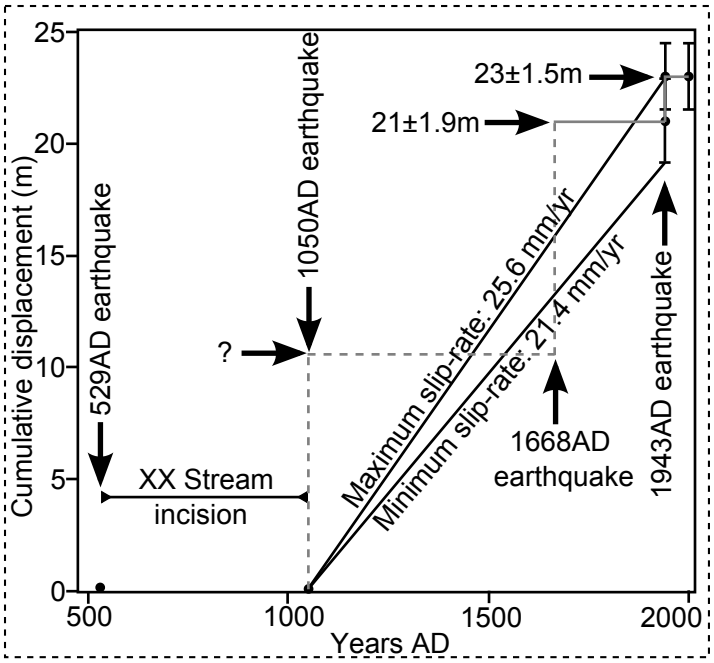

Table1

TABLE 1. RADIOCARBON DATING DATA

Sample number	Soil unit[#]	Trench wall	Lab number	Yield (%)	Mass (mg)	δ^{C13} (vpdp)	Fraction modern carbon (4d.p.)	CRA (yrsBP)* unrounded	CRA (yrsBP)* rounded**	Calibrated age (AD/BC)† unmodeled	Calibrated age (AD/BC)† modeled	Notes
Surface1	N/A	N/A	Aeon85	56	1.18	-22.6	0.8918 ± 0.0040	920 ± 36	920 ± 40	1027 AD – 1207 AD	N/A	Not used
More than one event has occured at this site prior to this record												
46	1a	E	Aeon60	58	1.23	-24.5	0.8854 ± 0.0076	978 ± 69	980 ± 70	899 AD – 1214 AD	N/A	Reworked
41	1b	E	Aeon123	43	1.31	-23.6	0.9270 ± 0.0036	609 ± 31	610 ± 30	1296 AD – 1404 AD	1291 AD – 1400 AD	
52	1b	W	Aeon206	59	1.08	-26.1	0.8905 ± 0.0036	932 ± 33	930 ± 35	1023 AD – 1175 AD	1023 AD – 1175 AD	
37	1b	E	Aeon58	3	1.10	-24.7	0.8309 ± 0.0048	1488 ± 46	1490 ± 50	434 AD – 650 AD	577 AD – 659 AD	
Event 1												
45	2a	E	Aeon59	21	1.16	-24.0	0.8375 ± 0.0040	1424 ± 38	1420 ± 40	565 AD – 663 AD	469 AD – 639 AD	
63	2a	W	Aeon122	47	1.19	-25.2	0.8024 ± 0.0030	1769 ± 30	1770 ± 30	137 AD – 376 AD	137 AD – 376 AD	
60	2b	W	Aeon121	52	1.09	-23.7	0.7829 ± 0.0031	1966 ± 31	1970 ± 30	42 BC – 118 AD	14 AD – 126 AD	
Event 2												
58	3a	W	Aeon120	7	1.13	-24.6	0.7824 ± 0.0030	1971 ± 31	1970 ± 30	44 BC – 113 AD	46 BC – 59 AD	
79	3a	W	Aeon119	59	1.13	-26.7	0.7630 ± 0.0027	2172 ± 28	2170 ± 30	361 BC – 119 BC	358 BC – 115 BC	
72	3a	W	Aeon61	58	1.13	-23.5	0.7784 ± 0.0030	2012 ± 31	2010 ± 30	93 BC – 65 AD	102 BC – 52 AD	
147	3b	E	Aeon116	1	0.41	-26.1	0.7007 ± 0.0065	2857 ± 74	2860 ± 70	1260 BC – 843 BC	N/A	Reworked
Event 3												
158	4a	E	Aeon62	49	0.80	-23.0	0.7429 ± 0.0050	2388 ± 54	2390 ± 50	753 BC – 385 BC	754 BC – 393 BC	
145	4a	E	Aeon115	31	0.94	-25.4	0.7340 ± 0.0027	2484 ± 30	2480 ± 30	771 BC – 417 BC	773 BC – 428 BC	
150	4b	E	Aeon113	52	1.05	-26.8	0.7168 ± 0.0029	2674 ± 32	2670 ± 30	896 BC – 799 BC	892 BC – 797 BC	
Event 4												
149	5a	E	Aeon114	49	1.07	-26.5	0.6829 ± 0.0033	3064 ± 38	3060 ± 40	1424 BC – 1216 BC	N/A	Reworked
123	5a	W	Aeon112	51	1.19	-24.2	0.7041 ± 0.0024	2819 ± 28	2820 ± 30	1048 BC – 904 BC	1008 BC – 906 BC	
14	5b	W	Aeon111	57	1.05	-24.7	0.7042 ± 0.0025	2818 ± 29	2820 ± 30	1050 BC – 901 BC	1051 BC – 928 BC	
Event 5												
97	6b	E	Aeon105	30	1.18	-24.5	0.6713 ± 0.0025	3202 ± 30	3200 ± 30	1521 BC – 1419 BC	1522 BC – 1418 BC	
9	6b	W	Aeon104	64	1.00	-24.9	0.6925 ± 0.0024	2952 ± 28	2950 ± 30	1265 BC – 1054 BC	1293 BC – 1087 BC	
115	6b	W	Aeon110	59	0.94	-26.6	0.6808 ± 0.0023	3089 ± 27	3090 ± 30	1428 BC – 1295 BC	1427 BC – 1295 BC	
90	6b	E	Aeon207	58	1.13	-25.8	0.6726 ± 0.0030	3186 ± 36	3190 ± 40	1523 BC – 1404 BC	1523 BC – 1403 BC	
96	6b	E	Aeon208	40	0.66	-26.4	0.6448 ± 0.0027	3525 ± 34	3520 ± 30	1941 BC – 1752 BC	1920 BC – 1747 BC	
Event 6												
113a	7a	E	Aeon 106	3	1.27	-23.6	0.6200 ± 0.0029	3841 ± 38	3840 ± 40	2461 BC – 2200 BC	2437 BC – 2145 BC	
113b	7a	E	Aeon107	6	1.21	-23.3	0.6360 ± 0.0022	3635 ± 28	3640 ± 30	2130 BC – 1916 BC	N/A	Not used
116	7a	W	Aeon210	40	1.17	-25.9	0.6377 ± 0.0030	3613 ± 38	3610 ± 40	2128 BC – 1884 BC	2132 BC – 1895 BC	
91	7a	E	Aeon103	42	0.82	-24.2	0.6891 ± 0.0032	2991 ± 37	2990 ± 40	1383 BC – 1116 BC	N/A	Contaminant
163§	7b	E	Aeon63	5	1.20	-24.1	0.5972 ± 0.0020	4141 ± 27	4140 ± 30	2873 BC – 2624 BC	N/A	Reworked
165	7b	E	Aeon212	4	1.32	-26.6	0.5827 ± 0.0022	4339 ± 31	4340 ± 30	3078 BC – 2895 BC	N/A	Reworked
Event 7												
167	8a	E	Aeon214	2	1.28	-25.7	0.5470 ± 0.0017	4846 ± 25	4850 ± 30	3695 BC – 3537 BC	N/A	Reworked
169	8a	E	Aeon64	10	0.55	-24.7	0.6090 ± 0.0032	3984 ± 42	3980 ± 40	2620 BC – 2347 BC	2624 BC – 2407 BC	
134	8b	W	Aeon102	63	1.06	-25.3	0.6233 ± 0.0032	3797 ± 41	3800 ± 40	2455 BC – 2050 BC	N/A	Contaminant
135	8b	W	Aeon211	53	1.32	-26.8	0.5927 ± 0.0019	4202 ± 26	4200 ± 30	2894 BC – 2679 BC	3175 BC – 2677 BC	

Note: Samples are in stratigraphic order and the rows labeled "Event" show the stratigraphic location of the event horizon.

Note: All dated samples are charcoal.

*Uncertainties for unrounded and rounded conventional radiocarbon age (CRA) are given at the 1σ (68.3%) confidence level.

†Unmodeled and modeled Calibrated ages are: - determined using Oxcal; http://c14.arch.ox.ac.uk/embed.php?File=oxcal.html accessed 2008.

- given at the 2σ (95.4%) confidence level (minimum and maximum bounds).

- calibrated with the Incal04 curve using the unrounded CRA.

- determined using the unrounded CRA, a departure from convention.

§δ^{C13} value not measured, the average value from this trench is used.

[#]The soil unit refers to unit labels on trench log Fig.4.

**Rounding follows convention (Stuiver and Polach, 1977).

Table2

TABLE 2. EVENT TIMING

Event	2σ Age range (years BC/AD)
E1:	549 AD – 651 AD
E2:	23 BC – 103 AD
E3:	609 BC – 185 BC
E4:	971 BC – 814 BC
E5:	1227 BC – 968 BC
E6:	2050 BC – 1777 BC
E7:	2556 BC – 2235 BC

Table3

TABLE 3. INTER-EVENT TIME

Interval	2σ range (years)
IET 1 - 2:	479 – 647
IET 2 - 3:	210 – 655
IET 3 - 4:	268 – 729
IET 4 - 5:	50 – 352
IET 5 - 6:	627 – 1012
IET 6 - 7:	271 – 702
SIET:	97 – 912
RI:	471 – 529

IET = Inter-event time

SIET = Summed inter-event time

RI = Reccurence interval

Supplemental file1

Click here to download Supplemental file: ES.1_sampleStrat.pdf

Supplemental file2

Click here to download Supplemental file: ES.2_Unit descriptions.txt

Supplemental file3

Click here to download Supplemental file: ES.3_Unconstrained_Oxcal_model.pdf